NUMERICAL SIMULATION OF ICE-DUST FLOW: EFFECTS OF GRAVITY AND CYCLIC HEAT ADDITION

A Thesis

by

ZHENYANG DONG

Submitted to the Graduate and Professional School of
Texas A&M University
in partial fulfillment of the requirements for the degree of

MASTER OF SCIENCE

Chair of Committee,	Elaine S. Oran
Committee Members,	Qingsheng Wang
	Waruna Kulatilaka
Head of Department,	Ivett Leyva

December 2021

Major Subject: Aerospace Engineering

ABSTRACT

One-dimensional numerical simulations are performed to analyze the ice-dust flow on cometary surfaces under the effect of gravity and cyclic heat addition. The objective is to investigate the ice formation process at the surface of the comet Tempel 1. The numerical model used in this thesis project is a gaseous-granular multiphase model, which describes the interactions of ice, dust, water vapor, and inert gas, and considers an external cyclic heat source and the sublimation and condensation processes between ice and water vapor. Simulations were conducted with different values of gravities. The results show that the ice and dust particles separate and lead to a final state with ice on the top and dust at the bottom. Ice particles are lifted from the ground under the effect of a cyclic heat source in the 0.001g case. Force evaluations show that particle behavior depends mainly on the magnitude of heat-induced forces and gravitational forces. Particle lifting and further separation between ice and dust only occur when the magnitude of heat-induced forces is larger than gravitational forces. These simulations support the hypothesis of ice-surface formation processes on T1.

CONTRIBUTORS AND FUNDING SOURCES

Contributors

This work was supported by a thesis committee consisting of my advisor, Professor Elaine Oran, and Professor Qingsheng Wang of the Department of Chemical Engineering and Professor Waruna Kulatilaka of the Department of Mechanical Engineering.

We thank Dr. Tony Farnham and Dr. Jessica Sunshine (University of Maryland) for suggestions and comments on the setup of test cases. We also thank Dr. Xiaoyi Lu and Dr. Xiao Zhang (Texas A&M University) for assistance in result analysis and comments on manuscript.

Funding Sources

Graduate study was supported by NASA Discovery Data Analysis Program 80NSSC18K1433.

TABLE OF CONTENTS

Page

ABSTRACT ii

CONTRIBUTORS AND FUNDING SOURCES iii

TABLE OF CONTENTS iv

LIST OF FIGURES vi

LIST OF TABLES viii

1. INTRODUCTION 1

2. PHYSICAL AND NUMERICAL MODEL 4

    2.1 Governing equations 4
    2.2 Phase change and cyclic heat-source 6
    2.3 Numerical algorithm 9

3. ANALYSIS BY FORCES 10

4. RESULTS 11

    4.1 Steady state without external heat input 11
        4.1.1 Problem setup and initialization 11
        4.1.2 Particle motion 12
        4.1.3 Evaluation of forces 15
    4.2 Particle behavior with cyclic heat input 18
        4.2.1 Particle motion 18
        4.2.2 Evaluation of forces 21

5. DISCUSSIONS 29

    5.1 Result interpretations in terms of ice surface formation on T1 29
    5.2 Parametric analysis of the test problem 30
    5.3 Evaluation of the multiphase model 31
        5.3.1 Granular frictional pressure 31
        5.3.2 Phase change and cyclic heat source 32
        5.3.3 Boundary conditions 32
        5.3.4 Numerical method 33

6. SUMMARY AND CONCLUSION 34

7. FUTURE WORK 35

REFERENCES 37

APPENDIX A. DETAILS OF PHYSICAL MODEL 44

LIST OF FIGURES

FIGURE Page

4.1 Simulation setup for the 1D test problem. 11

4.2 The evolution of ice and dust volume fraction as a function of time for different values of gravity. 13

4.3 The volume fraction profiles for ice and dust (a) at initial condition, (b) during the free-fall stage, and (c) during the separation stage. The gravity is 0.01g. The exact time for each figure is (a) $t = 0.0$s, (b) $t = 2.0$s, and (c) $t = 10.0$s. 14

4.4 The steady state volume fraction profiles for (a) ice particles, (b) dust particles, and (c) gas under different gravity. 14

4.5 Computed net force on ice and dust particles under different gravity: (a) 1g, (b) 0.1g, (c) 0.01g, and (d) 0.001g. 16

4.6 Computed Archimedes force, intergranular stress force, drag force, particle hindrance force, and gravitational force on ice and dust particles with 0.01g gravity. 17

4.7 Computed individual forces and net forces on ice and dust particles with 0.01g gravity during the separation stage at $t = 10.0$s. 18

4.8 The evolution of ice and dust volume fraction as a function of time for different gravity when the cyclic heat source is applied to the system. The phase change between ice and water vapor is turned off. 19

4.9 The evolution of ice and dust volume fraction as a function of time for different gravity when the cyclic heat source is applied to the system. The phase change between ice and water vapor is allowed. 20

4.10 Computed net force, Archimedes force, intergranular stress force, drag force, particle hindrance force, and gravitational force exerted on ice and dust particles as a function of time in 0.01g case when the cyclic heat source is being applied. The sublimation and condensation are turned off. 22

4.11 Computed net force, Archimedes force, intergranular stress force, drag force, particle hindrance force, and gravitational force exerted on ice particles as a function of time in 0.001g case when the cyclic heat source is being applied. The sublimation and condensation are turned off. 23

4.12 Computed individual forces and net forces on ice particles for different gravities. The sublimation and condensation are turned off. 24

4.13 The summation of Archimedes force and drag force on ice and dust particles as a function of time for different gravity when the cyclic heat source is being applied. The sublimation and condensation are turned off. 25

4.14 Computed profiles of (a) rate of change in ice volume fraction, (b) rate of latent heat transfer due to phase change, and (c) water vapor partial pressure in the case with 0.01g as the cyclic heat source being applied. (a) and (b) shares the same contour. 26

4.15 The summation of Archimedes force and drag force on ice and dust particles as a function of time under different gravity when the cyclic heat source is being applied. The sublimation and condensation processes are considered. 27

LIST OF TABLES

TABLE Page

3.1 Forces acting on particle type l. The equations for intergranular stress force, drag force, and particle hindrance force can be found in Appendix A. 10

4.1 Initial conditions for the 1D gaseous-granular multi-phase flow simulation 12

1. INTRODUCTION

Cometary nuclei have been an essential subject of research to understand the history of planetary formation. Variable solar radiation due to comet rotation and revolution creates a seasonal environment that leads to many special geological features [1]. The Deep Impact mission to 9P/Tempel 1 (T1) discovered several large, smooth patches on the cometary surface, which were identified as ice surfaces [2]. This geological terrain was found unique among existing observations, and has garnered significant interest in understanding its formation process.

One hypothesis for the development of the ice surface on T1 was proposed based on previous studies. Through Rosetta/OSIRIS observations of 67P/Churyumov-Gerasimenko (67P), it was found that the ice experiences cyclic sublimation and condensation processes that follow the local illumination conditions [3, 4]. Thin frost-like layers were identified as a result of ice recondensation and particle backflux from inner coma [5, 3, 4]. Mass transport on cometary surfaces has also been proven to be influenced significantly by seasonal effects due to outgassing [6, 7, 1]. The evolution of comets, in general, depends on surface material transport, which is governed by seasons [8, 9, 10]. Based on these considerations, it is hypothesized by Farnham $et\ al.$ [11] that the ice surface on T1 was formed due to external cyclic heat sources. They caused sublimation and condensation of ice and lift and deposition of particles, which led to the separation of ice and dust particles with ice on top of dust.

Different numerical models have been developed and tested for the simulation of comae and the cometary surfaces. The gas and dust activities in comae have been computed and analyzed using numerical models based on Navier-Stokes Equations or Direct Simulation Monte Carlo method [10, 12, 13, 14, 15, 16]. Sarid and Prialnik simulated the effect of the Deep Impact and the surface outburst on T1 using a thermal evolution model, which solves the conservation equations of mass and energy for gas and solid phases [17, 18]. Skorov analyzed the near-surface ice-dust interaction on 67P using a similar thermophysical model with additional considerations of particle aggregation [19, 20]. The momentum equation is omitted in these cometary surface models, and the particle

motion is simplified into flux models. The comae models treat the gas and dust in a similar way using rarefied gas dynamics [10], which are not directly applicable to cometary surfaces that involves dense granular system. This thesis presents a first attempt to utilize the gaseous-granular multiphase model on cometary surface simulations. This model solves the complete sets of mass, momentum, and energy conservation equations for gas and particles and considers gas and solid separately, thus a more detailed representation of ice-dust motion and interactions can be expected.

In the past decades, two types of approaches have been developed to model dense gas-solid systems: the Eulerian-Eulerian (EE) method and the Eulerian-Lagragian (EL) method. In both methods, the gas phase is treated as a continuum [21]. The EE method also treats the solid phase as a continuous phase, and the equations for the coupled gaseous-granular flow are developed based on the kinetic theory of granular flow and the theory of fluidization [22, 23]. In the EE framework, several existing multiphase models have been designed for different flow regimes, such as low-speed flows [24], high-speed flows with dilute particles [25], and high-speed flows with dense particles [26, 27]. The EL method treats gas as the carrier and simulates each particle individually [28]. In the EL framework, the particle-in-cell (PIC) method was developed, which is used to study incompressible dense-particulate flows [29, 30]. For these models, the complexity of calculations increases with the number of particle species (different densities or sizes) in the EE method and with the number of particles in EL method [31].

In a system with a large number of particles and only a few particle types, the EE framework provides a good balance between accuracy and computational cost [32]. There are many types of particles on a cometary surface, and their sizes and densities are unknown. In this study, we have assumed that all ice particles have one density and size, and all dust particles are of another density and size so that the system only contains two types of particles. Then it is efficient to use the EE method to model large clusters of ice and dust on cometary surfaces. The multiphase model developed by Houim and Oran [27] has been selected to study the surface flows because it calculates dense gas-solid system efficiently and accurately for simulations of dust dispersion [33] and subsurface comet explosions [34]. This project extends this model to describe a cyclic heat

source and phase changes between ice and water vapor due to sublimation and recondensation.

This project is motivated by the aforementioned hypothesis and tries to address the following questions: (1) What is the mechanism behind the separation of ice and dust particles? (2) How do different conditions, such as gravity and cyclic heat sources, affect the separation of ice and dust? To verify the hypothesis and answer these questions, the ice-dust flow on cometary surfaces is analyzed using a multiphase gaseous-granular model describing the interactions of ice, dust, water vapor, and inert gas. A model problem is selected, and initial conditions are subject to different gravities and cyclic heat sources. One-dimensional (1D) numerical simulations are performed in different gravities and cyclic heat sources to analyze the effect of lift and deposition of particles. The results are then interpreted for their implications to the ice-dust interactions on T1.

2.1 Governing equations

The gaseous-granular multiphase model developed by Hoium and Oran [27] and Lai $et\ al.$ [33] is a multi-dimensional, compressible model, which solves the Euler's equations of gas and granular fluid dynamics. The governing equations for 1D gaseous-granular multiphase flow are written with extensions to phase changes and cyclic heat sources. This section lists the conservation equations and equation of state for gas and granular phases. The model of phase change and cyclic heat sources are discussed in section 2.2 and the detailed explanations for all other physical quantities are included in Appendix A. This model is able to describe multiple types of particles with different sizes or densities simultaneously. The equations for mass, species, momentum, and energy for the gas phase in the 1D multiphase model are written as

$$\frac{\partial \alpha_g \rho_g}{\partial t} + \frac{\partial \alpha_g \rho_g v_g}{\partial x} = \sum_{l=1}^{N_s} \dot{M}_{jl}, \tag{2.1}$$

$$\frac{\partial \alpha_g \rho_g Y_j}{\partial t} + \frac{\partial \alpha_g \rho_g Y_j v_g}{\partial x} = \dot{M}_{jl} \ \text{ for } \ j = 1, ..., N_g, \tag{2.2}$$

$$\frac{\partial \alpha_g \rho_g v_g}{\partial t} + \frac{\partial \alpha_g \rho_g v_g^2}{\partial x} = -\alpha_g \frac{\partial p_g}{\partial x} + \alpha_g \rho_g g + \sum_{l=1}^{N_s} (f_{drag,gl} + v_{int} \dot{M}_{jl}), \tag{2.3}$$

$$\begin{aligned} \frac{\partial \alpha_g \rho_g E_g}{\partial t} + \frac{\partial \alpha_g v_g \left(\rho_g E_g + p_g\right)}{\partial x} &= -p_g \frac{\partial \alpha_g}{\partial t} + \alpha_g \rho_g v_g g \\ &+ \sum_{l=1}^{N_s} (f_{drag,gl} v_{s,l} - q_{conv,gl} + \phi_{visc,gl} - \phi_{slip,gl} + E_{gl,int} \dot{M}_{jl}), \end{aligned} \tag{2.4}$$

The equations for mass, momentum, pseudo thermal energy (PTE), and internal energy for the granular particle type l are written as,

$$\frac{\partial \alpha_{s,l}\rho_{s,l}}{\partial t} + \frac{\partial \alpha_{s,l}\rho_{s,l}v_{s,l}}{\partial x} = -\dot{M}_{jl}, \tag{2.5}$$

$$\begin{aligned}\frac{\partial \alpha_{s,l}\rho_{s,l}v_s}{\partial t} + \frac{\partial \alpha_{s,l}\rho_{s,l}v_{s,l}^2}{\partial x} = &-\frac{\partial p_{s,l,tot}}{\partial x} - \alpha_{s,l}\frac{\partial p_g}{\partial x} + \alpha_{s,l}\rho_{s,l}g \\ &- f_{drag,gl} - v_{gl,int}\dot{M}_{jl} - \sum_{m=1,m\neq l}^{N_s} f_{drag,lm},\end{aligned} \tag{2.6}$$

$$\frac{\partial \alpha_{s,l}\rho_{s,l}E_{s,l}}{\partial t} + \frac{\partial \alpha_{s,l}\rho_{s,l}E_{s,l}v_{s,l}}{\partial x} = -p_{s,l}\frac{\partial v_{s,l}}{\partial x} - \dot{\gamma}_l - \phi_{visc,gl} + \phi_{slip,gl} - E_{sl,int}\dot{M}_{jl}, \tag{2.7}$$

$$\frac{\partial \alpha_{s,l}\rho_{s,l}e_{s,l}}{\partial t} + \frac{\partial \alpha_{s,l}\rho_{s,l}e_{s,l}v_{s,l}}{\partial x} = q_{conv,gl} + \dot{\gamma}_l - e_{sl,int}\dot{M}_{jl} + \alpha_{s,l}\dot{Q}. \tag{2.8}$$

Here, α, ρ, v, and p are the volume fraction, density, velocity, and pressure for the gas and granular phases, denoted by subscripts g and s, respectively. The quantity Y is the gas species mass fraction. The quantities E_g, E_s, and e_s are the gas phase total energy, PTE, and the granular internal energy. The quantity N_g is the number of species in the gas phase, and N_s is the number of particle types. The subscript j denotes the gas species, and the subscripts l and m denotes different particle types. The rate of phase change between gas species j and granular particles l is represented by $\dot{M}_{jl}$. The phase change is a one-to-one process, and gas j and particles l represent the same substance in different phases. The subscript int indicates the gas-particle interface during phase change. The heat input and extraction to the granular particles are denoted by $\dot{Q}$. In this work, we consider two species of gas, water vapor and nitrogen, and two types of granular particles, dust and ice. The phase change only happens between water vapor and ice.

The gas phase is assumed ideal and the equation of state is used to relate the pressure, species composition, density and temperature,

$$p_g = \rho_g R_u T_g \sum_{j=1}^{N_g} \frac{Y_j}{M_{W_j}}, \tag{2.9}$$

where R_u is the universal gas constant, and M_{W_j} is the molecular weight for gas species j.

The gas-phase total energy is defined as

$$E_g = \sum_{j=1}^{N_g} Y_j \left(h_{f,j}^0 + \int_{T_0}^{T_g} C_{p,j} dT \right) - \frac{p_g}{\rho_g} + \frac{v_g^2}{2}, \tag{2.10}$$

where h_f^0 is the formation enthalpy at reference temperature T_0, and C_p is the constant-pressure specific heat. Granular PTE describes the energy due to particle random translational motion. It is proportional to the granular pseudo temperature ($\theta_{s,l}$), which represents the mean square of the particle velocity fluctuations due to collisions,

$$E_{s,l} = \frac{3}{2}\theta_{s,l}. \tag{2.11}$$

The internal energy of particles is defined as

$$e_{s,l} = e_{f,sl}^0 + \int_{T_0}^{T_{s,l}} C_{v,sl} dT, \tag{2.12}$$

where $e_{f,s}^0$ is the internal energy of formation at T_0, and $C_{v,s}$ is the constant-volume specific heat. In this model, T_0 is taken as 0K.

2.2 Phase change and cyclic heat-source

Here we describe a model for $\dot{M}_{jl}$ to account for the rate of phase change between water vapor (j) and ice particles (l) at different temperatures and pressure conditions. It is assumed that the phase change processes do not change the particle shape, diameter, or inner particle temperature. The mass gain or loss in the ice particle cloud is treated as adding or losing ice particles of the same size and shape.

The theory of an evaporating sphere is developed based on the transfer of mass and heat between the sphere and the ambient gas [35]. The governing equations for the mass diffusion and heat conduction of a single ice particle can be written as [36]

$$-\dot{M}_0 = \frac{dm_l}{dt} = 2\pi D_j r_l (\rho_j - \rho_{int,j}), \tag{2.13}$$

$$L_s \frac{dm_l}{dt} = 2\pi K_g r_l (T_g - T_{int}), \tag{2.14}$$

where D_j is the diffusion coefficient of water vapor in air, r_l is the particle radius, ρ_j and $\rho_{int,j}$ are the water vapor density at far field and at the ice-vapor interface, L_s is the latent heat in phase change, and K_g is the thermal conductivity of air. The saturation pressure $p_{sat,j}$ is a function of temperature by the Buck equation [37],

$$p_{sat,j}(T_g) = 611.15 \exp\left(\left(23.036 - \frac{T_g - 273.15}{333.7}\right)\left(\frac{T_g - 273.15}{6.67 + T_g}\right)\right), \tag{2.15}$$

and the saturation density $\rho_{sat,j}$ can be obtained through ideal gas law. Assuming $(T_g - T_{int})$ is small and $\rho_{int,j} = \rho_{sat,j}(T_{int})$, $\dot{M}_0$ can be derived as [35]

$$\dot{M}_0 = \frac{\pi d_l \left(1 - \rho_j / \rho_{sat,j}(T_g)\right)}{\frac{L_s}{KT_g}\left(\frac{L_s M_{W_l}}{R_u T_g} - 1\right) + \frac{1}{D_j \rho_{sat,j}(T_g)}}. \tag{2.16}$$

Although the above theory was originally developed for sphere evaporation [36], Eq (2.13) and (2.14) are also applicable to condensation. Therefore, $\dot{M}_0$ can be treated as the mass rate of change for both sublimation and condensation of a single particle. The phase change model is then

$$\dot{M}_{jl} = n_l \dot{M}_0, \tag{2.17}$$

which gives the total rate of phase change in a unit volume.

This phase change model can be validated using existing experimental results, where an ice particle of 4.4 μL got fully sublimated in 6 hours in a -10°C, 4.8% relative humidity environment [38]. Under the constant particle diameter assumption, the time of sublimation is calculated as 243 minutes using Eq. (2.16). This result is in the same order of magnitude as the experimental data but with some deviations, which can be explained by the experimental setup. In the experiment, the ice particle was placed on the glass and part of its surface are unexposed to the air. Therefore, the rate of sublimation was lower than theory since the interface area between ice and air is smaller.

On the other hand, the constant diameter assumption may also cause deviations, and calibrations may be needed in the future.

The interface values during phase change are defined according to the phase that is losing mass. The latent heat of phase change is extracted from or released only to the gas phase,

$$v_{gl,int} = \begin{cases} v_{s,l}, & \text{if } \dot{M}_{jl} > 0, \\ v_g, & \text{if } \dot{M}_{jl} < 0. \end{cases} \quad E_{gl,int} = \begin{cases} e_{s,l} + E_{s,l} + v_{s,l} \cdot v_{s,l}/2, & \text{if } \dot{M}_{jl} > 0, \\ e^0_{f,sl} + \int_{T_0}^{T_g} C_{v,sl} dT, & \text{if } \dot{M}_{jl} < 0. \end{cases}$$

$$E_{sl,int} = \begin{cases} E_{s,l}, & \text{if } \dot{M}_{jl} > 0, \\ 0, & \text{if } \dot{M}_{jl} < 0. \end{cases} \quad e_{sl,int} = \begin{cases} e_{s,l}, & \text{if } \dot{M}_{jl} > 0, \\ e^0_{f,sl} + \int_{T_0}^{T_g} C_{v,sl} dT, & \text{if } \dot{M}_{jl} < 0. \end{cases} \tag{35a-d}$$

Here, $\dot{Q}$ is the rate of cyclic heat input and extraction, which models the effect of cyclic solar radiation. We assume $\dot{Q}$ is applied directly to all granular particles. As the granular temperature changes cyclically, the ambient gas temperature changes as well, which alters the process of sublimation and condensation by changing the water vapor saturation pressure. The heat radiation process is simplified, and $\dot{Q}$ is represented using a sinusoidal model,

$$\dot{Q} = C \frac{\pi Q_{tot}}{\tau} \cos\left(\frac{2\pi}{\tau} t\right), \tag{2.19}$$

where τ is the period of heat cycle and Q_{tot} is the total amount of energy input or extraction in a half-cycle. During heating or cooling, the energy input or extraction is a fixed value controlled by Q_{tot}, and the net energy change in a complete cycle is zero. The quantity C is the heat distribution coefficient, which is a function of location. The effect of the solar radiation is the largest on the surface layer and becomes smaller as the heatwave penetrates deeper into the interior [10]. Here, a linear function is assumed for C. Details for the setup of C are shown in section 4.2.

2.3 Numerical algorithm

The numerical method for solving the multiphase model is based on the works of Houim and Oran [27] and Lai $et\ al.$ [33]. The primitive variables are reconstructed using the second-order TVD MUSCL scheme with a minmod slope limiter. The gas-phase fluxes are computed using the second-order Kurganov and Tadmor (KT) central scheme [39]. The granular-phase fluxes are computed using the modified ASUM^{+}-up scheme [27], which increases diffusion and dissipation in densely packed regions. The hyperbolic fluxes are integrated using the strong stability-preserving second-order Runge-Kutta method.

A Strang operator splitting scheme is adopted to split the integration of hyperbolic fluxes and source terms. The integration of source terms is further split into three components: (1) drag force, particle-hindrance force, and heat convection, (2) PTE production, transfer, and dissipation, and (3) phase change and external heat input. The advancement of (1) and (2) are completed through analytical integration, and the details can be found in Houim and Oran's work [27] and Pelanti and Leveque's work [25]. The integration of (3) is calculated using the first-order forward Euler method.

3. ANALYSIS BY FORCES

In this project, we study the granular flow mechanism by analyzing the forces. Table. 3.1 identifies five different forces acting on the particles in 1D: the Archimedes force, the intergranular stress force, the drag force, the particle-hindrance force, and gravitational force [33]. Since these forces determines the ice-dust flow behavior, evaluating and comparing these forces helps explain how cyclic heat source affects particle motion. Here, we briefly describe the effect of each force on particle behavior based on their equations listed in Appendix A.

The Archimedes force is caused by the gas pressure acting on the particles, and it acts to move the particles from the high-pressure region to the low-pressure region. The intergranular stress force represents the contact forces among particles. This force prevents particles from entering dense regions because the intergranular stress ($p_{s,l,tot}$) increases exponentially with particle volume fraction when it is close to the packing limit. The drag force is induced from the velocity differences between the gas and particles, and it acts to equalize the gas and particle velocities. The particle-hindrance force is a drag-like force, which tries to equalize the velocities of two different types of particles. The gravitational force is acting downward. More detailed explanations of these forces can be found in Lai's work [33].

Table 3.1: Forces acting on particle type l. The equations for intergranular stress force, drag force, and particle hindrance force can be found in Appendix A.

(1) Archimedes force	$-\alpha_{s,l}\frac{\partial p_g}{\partial x}$	
(2) Intergranular stress force	$-\frac{\partial p_{s,l,tot}}{\partial x}$	Eq. (A.1) $-$ (A.6)
(3) Drag force	$K_{gl}(v_{s,l} - v_g)$	Eq. (A.7) $-$ (A.10)
(4) Particle-hindrance force	$K_{lm}(v_{s,l} - v_{s,m})$	Eq. (A.11) $-$ (A.12)
(5) Gravitational force	$\alpha_{s,l}\rho_{s,l}g$	

4. RESULTS

Here we present results of using the 1D multiphase model to solve the evolution of mixed ice and dust particles subject to different gravities and cyclic heat sources. These results are separated into two parts, steady-state results without any external heat input and particle lifting with cyclic heat input. The steady-state results are the starting point for the simulations with cyclic heat sources. In each part of the results, we present the particle motion first and then use force evaluation to analyze the particle behavior.

4.1 Steady state without external heat input

4.1.1 Problem setup and initialization

The initial setup for the 1D simulations is illustrated in Fig. 4.1. The schema is in 2D for clarity, and we only consider the interactions in the vertical direction. The computational domain

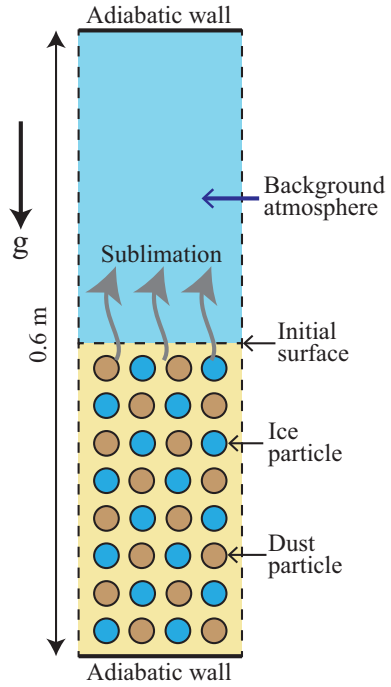

Figure 4.1: Simulation setup for the 1D test problem.

Table 4.1: Initial conditions for the 1D gaseous-granular multi-phase flow simulation

	p_g (atm)	ρ_g ($\mathrm{kg/m^3}$)	T_g (K)	Y_{vapor}	v_g ($\mathrm{m/s}$)	$\alpha_{s,ice}$	$v_{s,ice}$ ($\mathrm{m/s}$)	$E_{s,ice}$ ($\mathrm{m^2/s^2}$)	$\alpha_{s,dust}$	$v_{s,dust}$ ($\mathrm{m/s}$)	$E_{s,dust}$ ($\mathrm{m^2/s^2}$)
Upper	1.0	1.3655	250	0.0	0	0	0	0	0	0	0
Lower	1.0	1.3655	250	0.0	0	0.2	0	0	0.2	0	0

is divided into two equally long regions, where the upper region is background gas and the lower region is a homogeneous mixture of gas, ice, and dust. The initial values of the primitive variables for each region are given in Table. 4.1. The top and bottom boundaries are adiabatic walls that keep the total mass and energy conserved in the system. Gravity acts downward. Four different values of gravity were tested: 1g, 0.1g, 0.01g, and 0.001g, where g is the earth's gravitational acceleration.

The densities of the ice and dust particles are $1000\,\mathrm{kg/m^3}$ and $2500\,\mathrm{kg/m^3}$, respectively. The diameters of ice and dust particles are assumed to be $500\,\mu\mathrm{m}$. The initial vapor pressure is $0.0\,\mathrm{Pa}$ and the relative humidity is 0%.

A resolution test was conducted using the case in 0.01g. This test was computed using 200, 400, and 800 cells. The particle motions in different resolutions are the same, and the results show convergence. In the following simulations, we used 200 uniform grid points, and the Courant–Friedrichs–Lewy (CFL) number was 0.3.

4.1.2 Particle motion

Here we analyze the particle motion and the final steady-state under the effect of gravity. It is expected that the particles will fall to the ground and be bound by gravity. These test problems are used to ensure the model represents what should be obvious, and the results agree with our expectations. These analyses will also help us understand more complex results when external heat sources are added.

Fig. 4.2 shows the evolution of ice and dust volume fractions for different values of gravity.

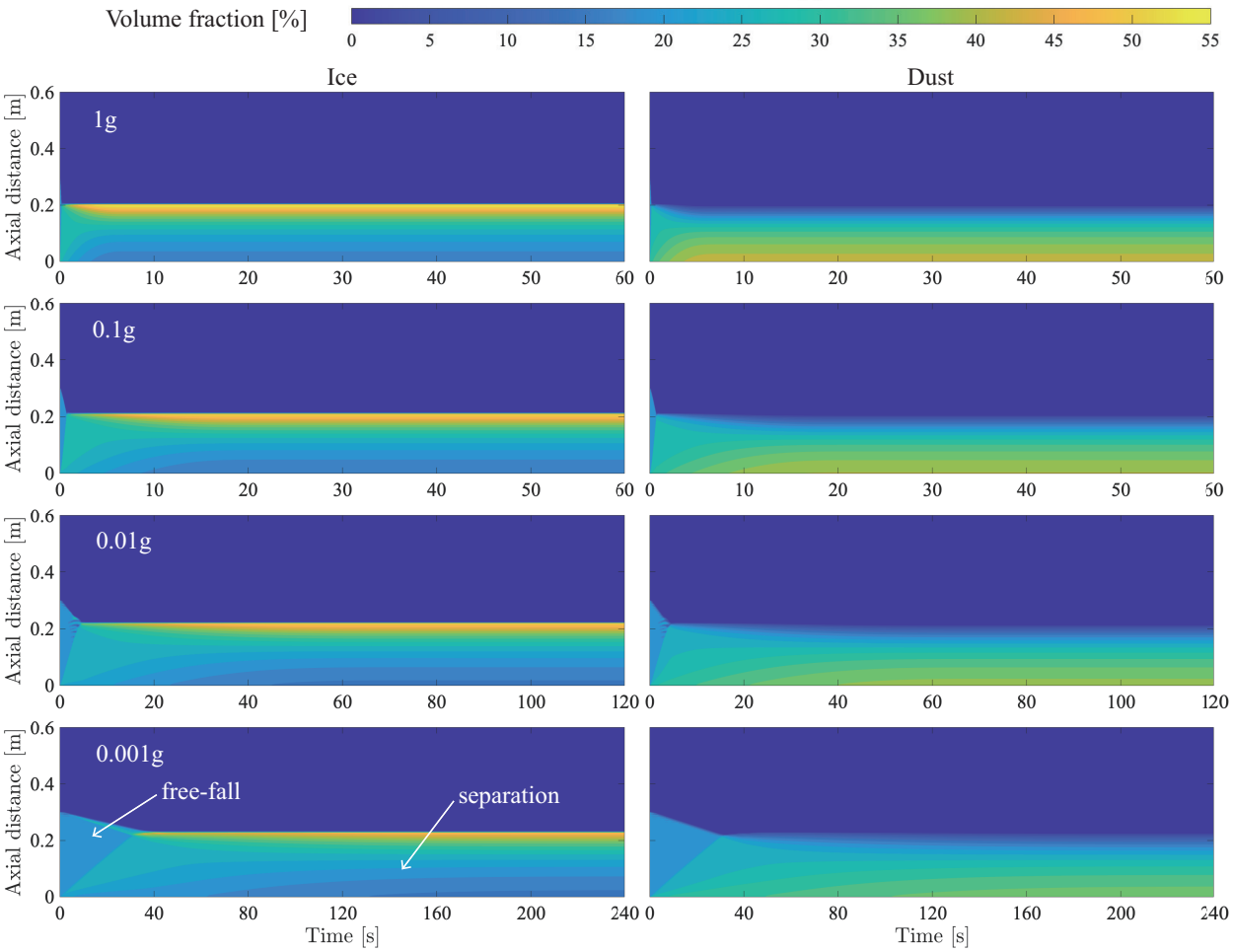

Figure 4.2: The evolution of ice and dust volume fraction as a function of time for different values of gravity.

With the given initial conditions and no external heat input, the evolution of particle volume fractions has two stages: the free-fall stage and the separation stage.

In the free-fall stage, the ice and dust particles fall under gravity and form a densely packed layer. Fig. 4.3(a) shows the volume-fraction profiles for ice and dust at $t = 0.0$s. Initially, the ice and dust particles in the lower half of the domain are not densely packed since the total volume fraction is 40%. Once the simulation begins, the ice and dust particles move downward together due to gravity and become densely packed at the bottom with a total volume fraction around 60%. The dense region grows in height as it takes in more particles. Fig. 4.3(b) shows the volume-fraction profiles during the free-fall stage using the 0.01g case as an example. At that time, a dense

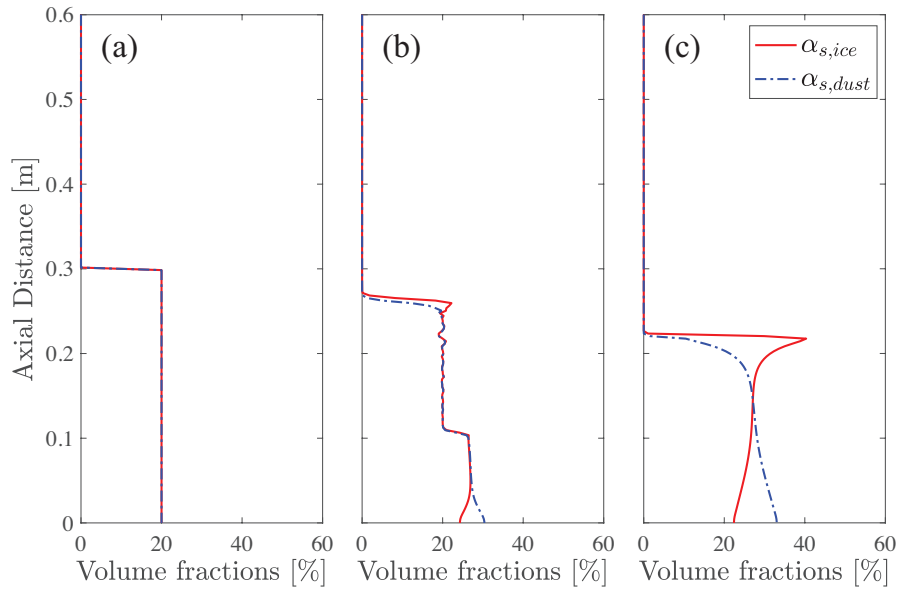

Figure 4.3: The volume fraction profiles for ice and dust (a) at initial condition, (b) during the free-fall stage, and (c) during the separation stage. The gravity is 0.01g. The exact time for each figure is (a) $t = 0.0$s, (b) $t = 2.0$s, and (c) $t = 10.0$s.

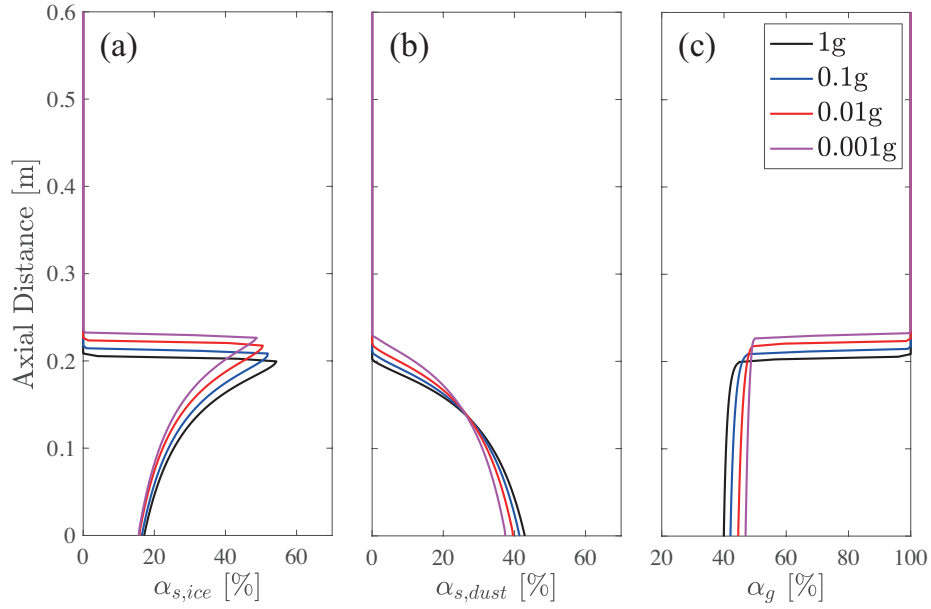

Figure 4.4: The steady state volume fraction profiles for (a) ice particles, (b) dust particles, and (c) gas under different gravity.

particle layer has been formed with a height of 0.11m. For particles initialized at 0.3m, the free-fall distance is around 0.1m. When the gravity is weaker, the time needed in the free-fall stage is longer.

In the separation stage, the particles remain densely packed on the ground, but the ice particles move upward, and the dust particles move downward. The system gradually reaches a steady state with ice on the top and dust at the bottom. Fig. 4.3(c) the volume-fraction profiles during the separation stage. The time needed for the system to reach a steady state is longer when the gravity is weaker.

At the final steady-state, the particles have zero velocity, and it will be shown that the force balance is achieved for each type of particle. Fig. 4.4 shows the steady-state volume-fraction profiles for ice, dust, and gas for different gravities. These profiles are similar, with more dust accumulating at the bottom and more ice accumulating at the top surface of the pile. When the gravity is stronger, the height of the dense particle pile is lower, and the particles are more densely packed.

4.1.3 Evaluation of forces

We now analyze the forces acting on different types of particles starting at the initial condition until the steady-state is reached. Fig. 4.5 presents the net forces on ice and dust under different gravities. In the free-fall stage, the particles experience downward net forces. In the dense region, the net forces act upward on ice particles and downward on dust particles. The net forces approach zero as the ice and dust gradually separate and reach a steady state. The stronger the gravity is, the larger the magnitude of net forces is.

Fig. 4.6 presents profiles of the five different forces for 0.01g as an example. In the free-fall stage, the gravitational force is dominant. Upward Archimedes force and drag force are acting on free-falling particles because the gas is compressed by incoming particles. At the end of the free-fall stage, the Archimedes force and drag force become negligible. For the particles that have reached the dense region, an upward intergranular stress force acts on them to counteract the gravitational force.

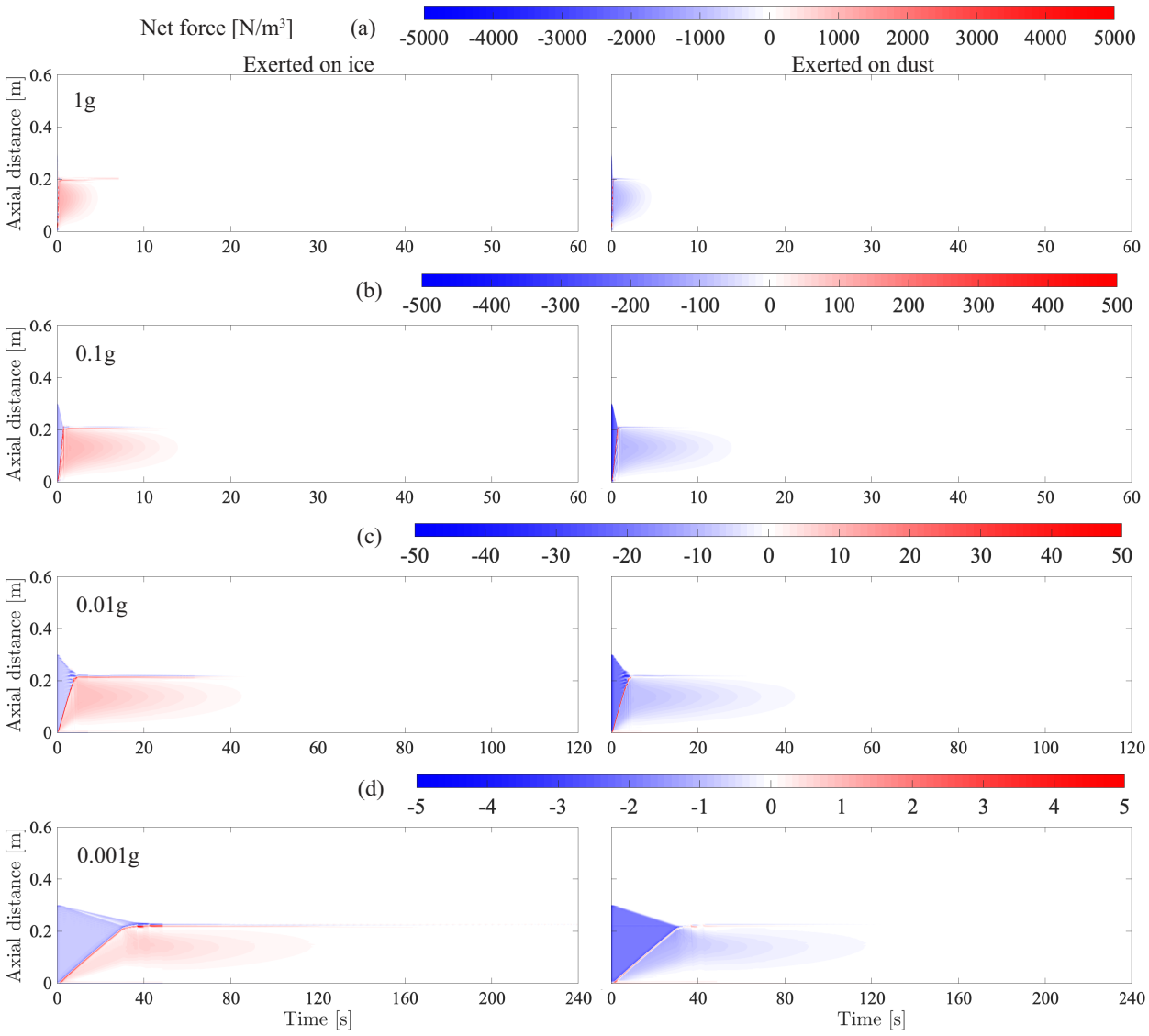

Figure 4.5: Computed net force on ice and dust particles under different gravity: (a) 1g, (b) 0.1g, (c) 0.01g, and (d) 0.001g.

In the separation stage, the ice particles are pushed upward, and the dust particles are forced downward. Fig. 4.7 shows the force profiles at $t = 10.0$s for 0.01g case. For both ice and dust particles, the gravitational force and intergranular stress force are dominant, and the particle motion depends on the magnitude of these two forces. Due to the difference in density and volume-fraction profiles for ice and dust, the forces acting on the ice and dust particles are different, and this causes the ice and dust to move in different directions. The intergranular stress force on ice particles is

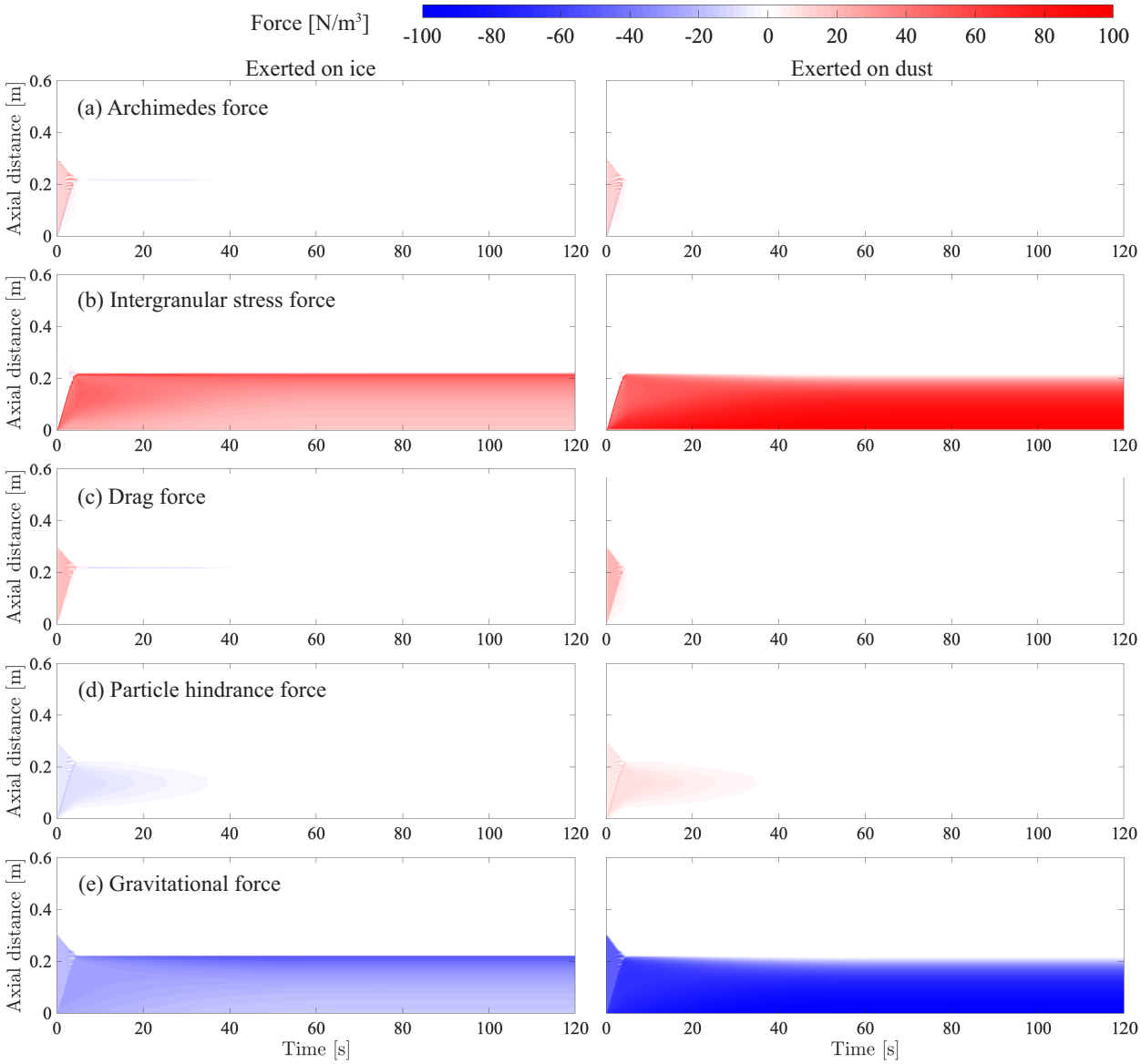

Figure 4.6: Computed Archimedes force, intergranular stress force, drag force, particle hindrance force, and gravitational force on ice and dust particles with 0.01g gravity.

larger than the gravitational force, and the opposite applies to dust particles, which leads to the separation. The particle hindrance force appears to slow down the relative motion of ice and dust particles, but it only creates limited effects due to its small magnitude. At the steady-state, only intergranular stress and gravitational forces exist in the system, and they are fully balanced.

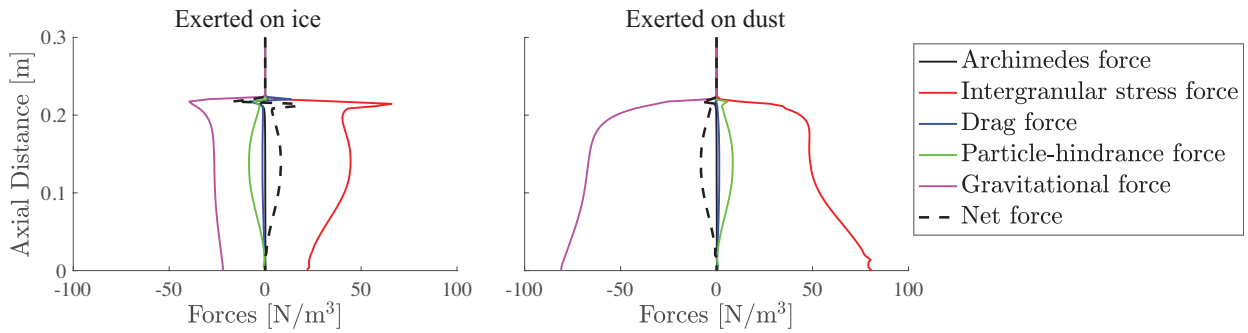

Figure 4.7: Computed individual forces and net forces on ice and dust particles with 0.01g gravity during the separation stage at $t = 10.0$s.

4.2 Particle behavior with cyclic heat input

Now, we show how gravity and a cyclic heat source affect the ice and dust particle motion. These tests demonstrate the ability of this model to reproduce the essential physical processes in cometary surface evolutions, namely, sublimation and condensation of ice and lifting and redeposition of particles.

4.2.1 Particle motion

With the steady-state results as starting points, the same cyclic heat source is applied for each value of gravity. The parameters of the heat source are set as $Q_{tot} = 1 \times 10^8 \mathrm{J/m^3}$ and $\tau = 20$s, which were chosen to change the temperature between 230K and 270K in a time scale that is similar to free-fall. The heat distribution coefficient C is set as a linear function with $C = 1$ at the top of the particle pile and $C = 0.5$ at the bottom. For each case, the simulation is conducted for 120s, which includes six heating cycles. Simulations are conducted both with and without the phase change between water vapor and ice to analyze the effect of cyclic heat source and phase change separately.

Consider first the particle flow caused by the heat source where there is no phase change allowed between water vapor and ice. Fig. 4.8 shows the evolution of the volume fraction of ice and dust when the cyclic heat source is being applied. The results for the 1g, 0.1g, 0.01g cases are similar, and the results for the 0.001g case are different from the others. In the first three cases,

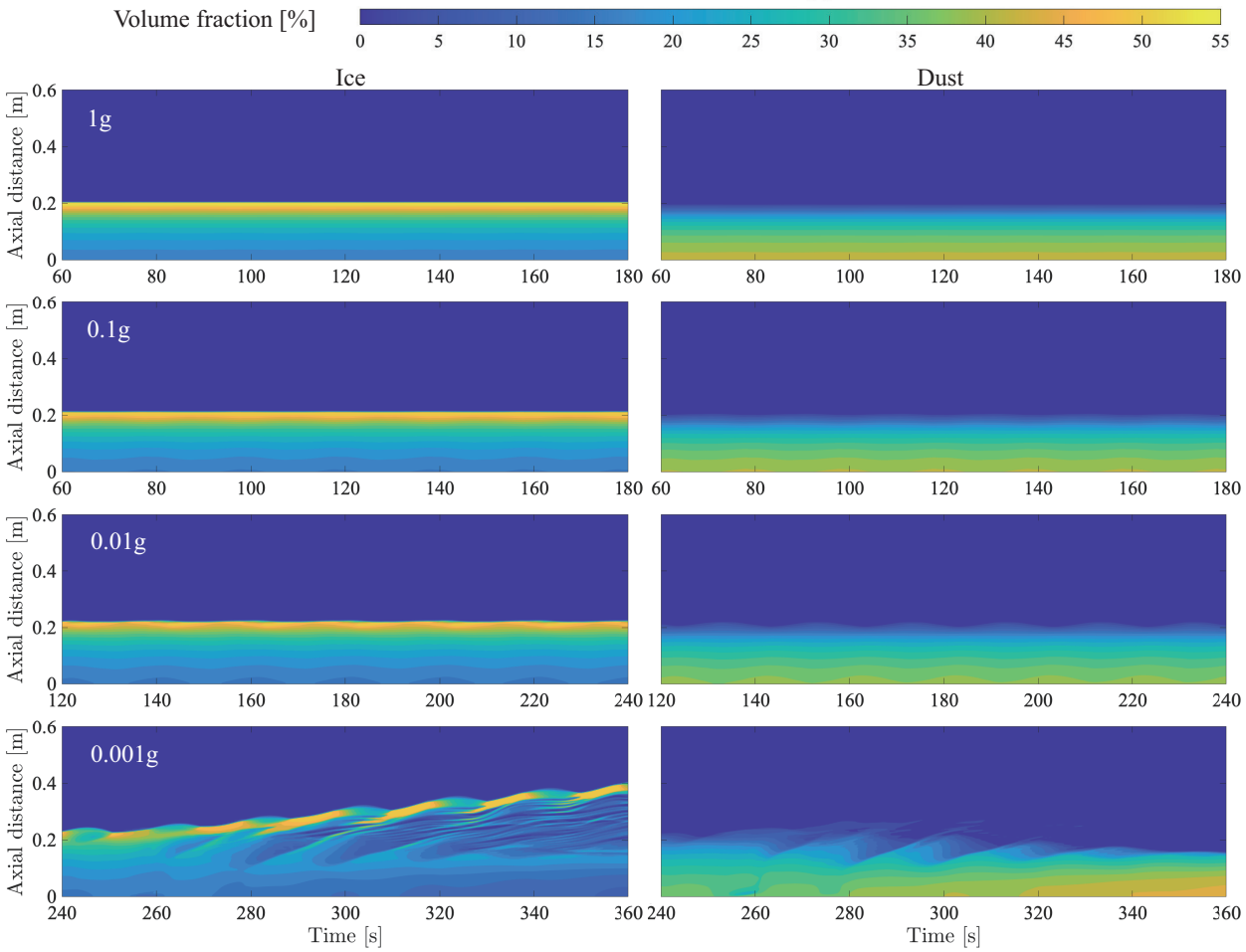

Figure 4.8: The evolution of ice and dust volume fraction as a function of time for different gravity when the cyclic heat source is applied to the system. The phase change between ice and water vapor is turned off.

the particles experience periodic upward and downward motions driven by the thermal fluctuations while gravitationally bound to the cometary surface. The period of these motions is the same as the period of the heat source. The stronger the gravity is, the less susceptible the particles are to the external thermal effects. The periodic variations in ice and dust volume fractions are the largest at 0.01g and not observable at 1g. At 0.001g, the particles also experience upward and downward motions, but in general, the ice particles are lifted from the particle pile, and dust particles sink to the bottom. The majority of the lifted ice particles cluster into a 0.2m layer whose volume fraction ranges from 35% to 50%. In this case, the ice particles overcome the gravity and rise to 0.4m. Ice

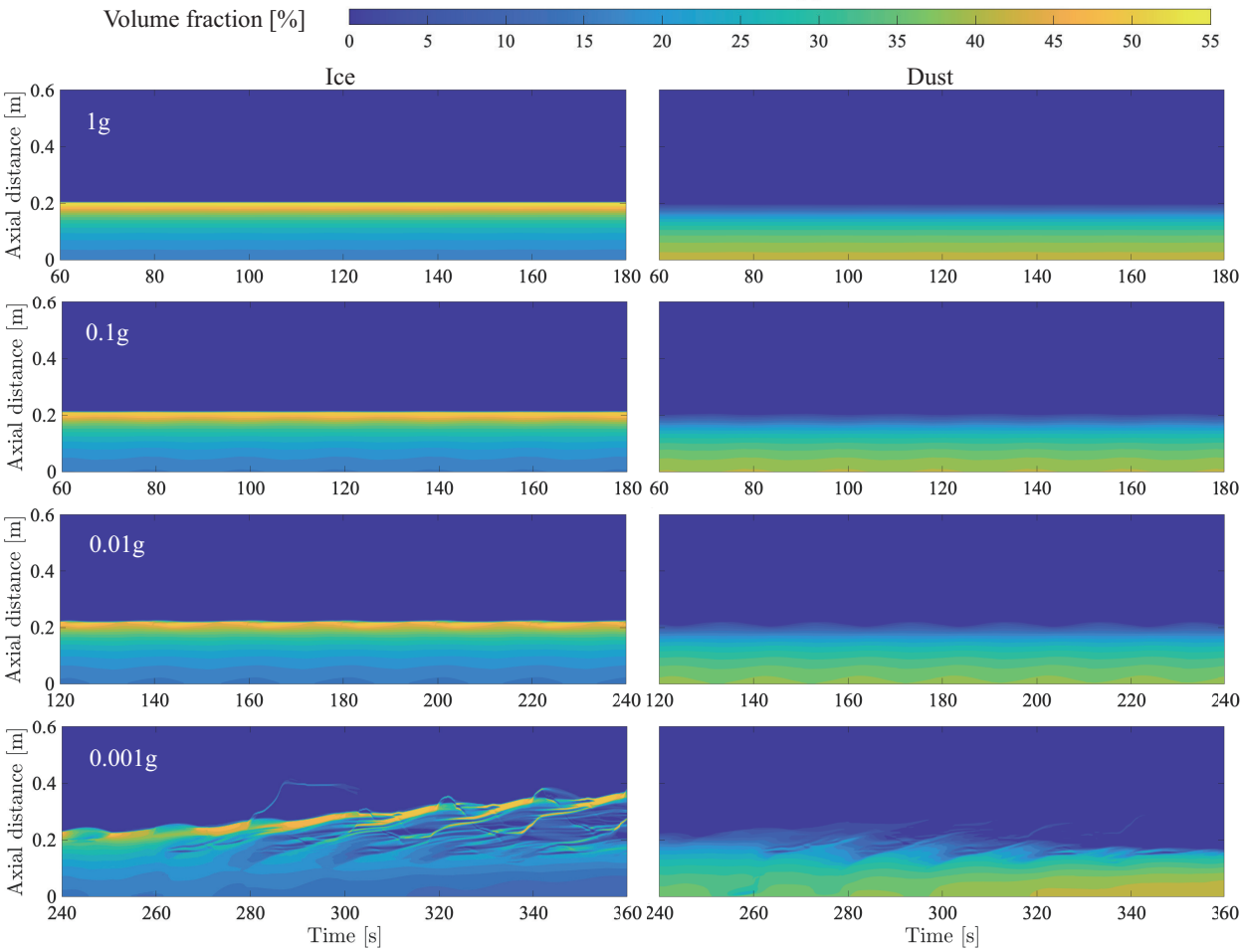

Figure 4.9: The evolution of ice and dust volume fraction as a function of time for different gravity when the cyclic heat source is applied to the system. The phase change between ice and water vapor is allowed.

and dust particles are further separated.

Fig. 4.9 shows the ice and dust volume fractions during the application of the heat source with the ice-vapor phase change allowed. As with the case without phase change, there are no observable variations for 1g, and there are periodic variations for 0.1g and 0.01g. At 0.001g, the ice is lifted from the ground, and ice and dust are further separated. The particle behavior at 0.001g with phase change is slightly different from the case without phase change. In the case with phase change, some ice particles rise suddenly. In general, the particle behavior is similar to the cases without phase change shown in Fig. 4.8. In the given scenario, the sublimation and condensation

processes only have a minor effect on the particle behavior compared to the heat source.

4.2.2 Evaluation of forces

Particle motions are caused by the forces generated by the heat source. As the particles are heated and cooled cyclically, the gas temperature changes cyclically. Because the energy in the heat source is not distributed uniformly and different types of particles have different specific heat, the gas temperature varies with location, which causes a gas pressure gradient. The pressure gradient generates the Archimedes force and also causes the gas to move. As a result, a drag force is also generated on particles in the direction of the gas velocity. The Archimedes force and the drag force caused by gas pressure gradient have the same direction, and below, it is shown that they also are of the same order of magnitude. These two heat-induced forces are the leading cause of particle motion.

Fig. 4.10 shows the net force and all five separate forces acting on particles at 0.01g when the cyclic heat source is applied. This case is chosen to demonstrate the force variations under the effect of cyclic heat source because all individual forces have a similar order of magnitude. As the temperature changes periodically, the forces on each type of particle also changes periodically. The heat-induced forces (Archimedes force and drag force) have similar profiles. In this case, they are not strong enough to overcome gravity, so they only perturb the original force balance and cannot lift the particles. Upward heat-induced forces counteract some of the gravitational force, and the local intergranular stress force decreases. During the entire process, the intergranular stress force stays positive and supports the weight of the particles. The changes in heat-induced forces and intergranular stress force lead to nonzero net forces, which cause the particles to move upward and downward cyclically.

Fig. 4.11 shows the forces on ice particles in 0.001g case. Only the forces exerted on ice are shown to describe how ice particles are lifted. In this case, the gravity is feeble, and the magnitude of heat-induced forces is larger than the gravitational force. The intergranular stress force is generated to resist particle compaction by counteracting the heat-induced forces. In the dense region (0 to 0.2m), the upward intergranular stress force balances the downward heat-induced forces, and

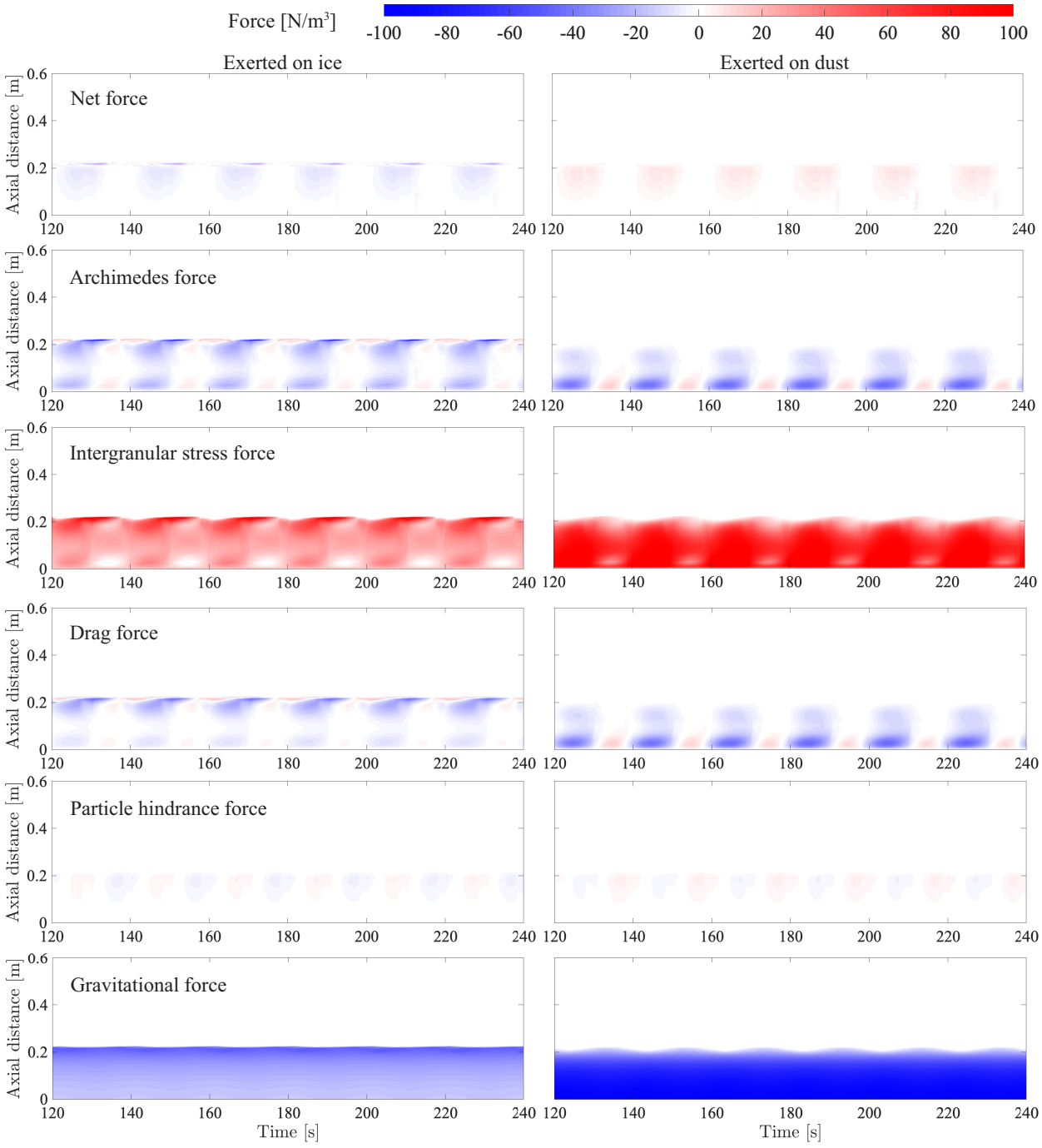

Figure 4.10: Computed net force, Archimedes force, intergranular stress force, drag force, particle hindrance force, and gravitational force exerted on ice and dust particles as a function of time in 0.01g case when the cyclic heat source is being applied. The sublimation and condensation are turned off.

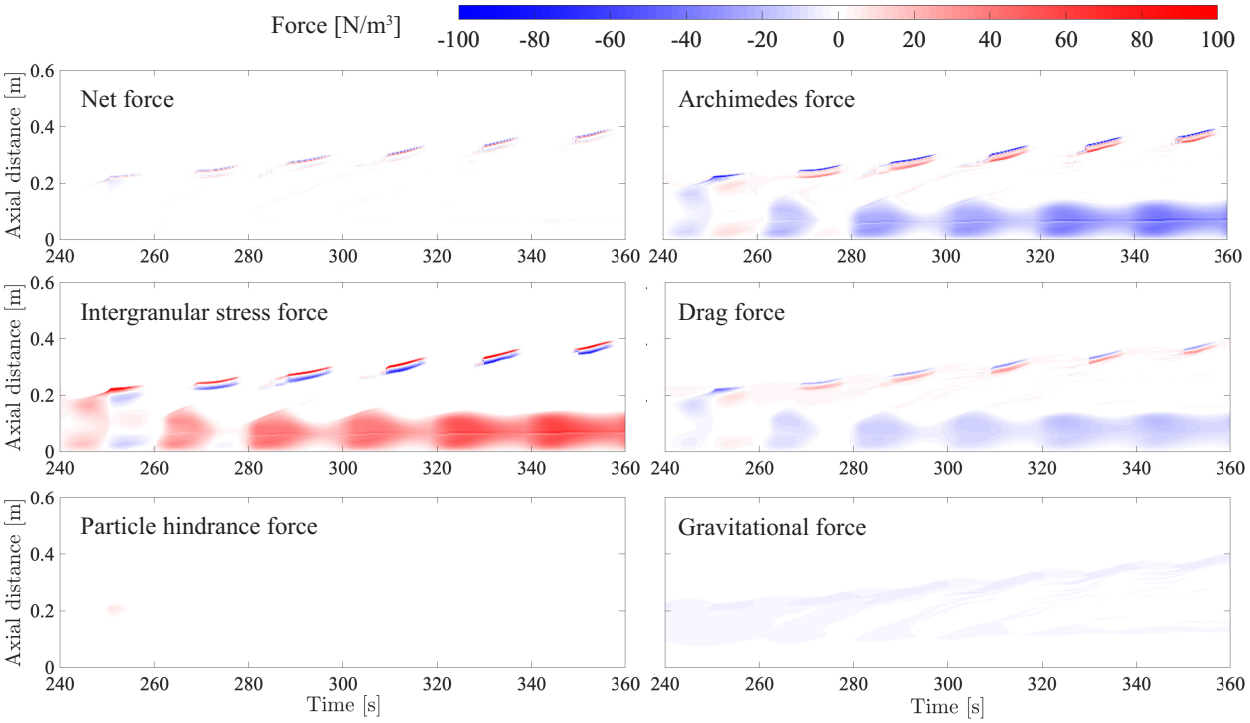

Figure 4.11: Computed net force, Archimedes force, intergranular stress force, drag force, particle hindrance force, and gravitational force exerted on ice particles as a function of time in 0.001g case when the cyclic heat source is being applied. The sublimation and condensation are turned off.

the net force is close to zero. In the region where ice is lifted (0.2m to 0.4m), large heat-induced forces are exerted on ice for half a period in every heat cycle. They are acting upward near the bottom of the lifted ice cluster and acting downward near the top, resulting in a compressing effect on the lifted particle layer. The intergranular stress force is acting in opposite directions as the heat-induced forces counteract the compression, which cancels out part of the heat-induced forces. The net force pushes the lifted ice layer upward while keeping the layer compressed. This leads to the observed phenomena where ice is lifted higher and higher, and the thickness and volume fraction of the lifted ice layer vary periodically.

Fig. 4.12 shows the force profiles at selected times for different gravities to compare the forces in different cases. Since the heat-induced forces vary with heating and cooling, the forces are compared when the heat-induced forces are the strongest. In the 1g, 0.1g, and 0.01g cases, the force profiles at the end of the first heat cycle are shown. The heat-induced forces are weaker

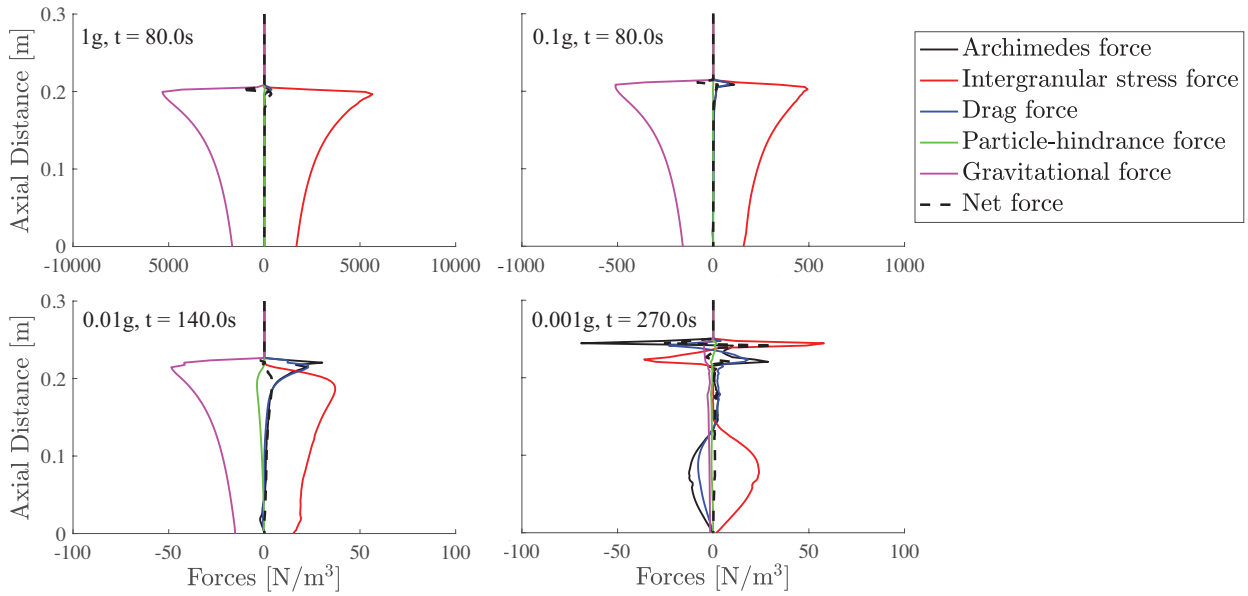

Figure 4.12: Computed individual forces and net forces on ice particles for different gravities. The sublimation and condensation are turned off.

than the gravitational force, which is balanced by the intergranular stress force. In the 0.001g case, the force profile at the middle of the second heat cycle is shown. The gravitational force is negligible, and the particle motion is governed by heat-induced forces and the intergranular stress force. The particle-hindrance force is negligible in all cases. Combining the information in Fig. 4.10, Fig. 4.11, and Fig. 4.12, it is found that the intergranular stress force always has a similar magnitude as the largest force in the system. It counteracts the gravitational force or the heat-induced force to resist particle compaction, which creates a decelerating effect on particle motion. Therefore, the intergranular stress force is not a cause of particle motion, and its magnitude depends on the magnitude of heat-induced forces and the gravitational force.

Fig. 4.13 presents the total heat-induced forces when applying the cyclic heat source in cases with different gravities. This figure shows that the order of magnitude for the heat-induced forces, around $100\mathrm{N/m^3}$, is the same regardless of the gravity. When the gravity is 1g, 0.1g, or 0.01g, the heat-induced forces are not strong enough to overcome the gravitational force so that the particles cannot be lifted from the ground. In these cases, the direction of the heat-induced forces

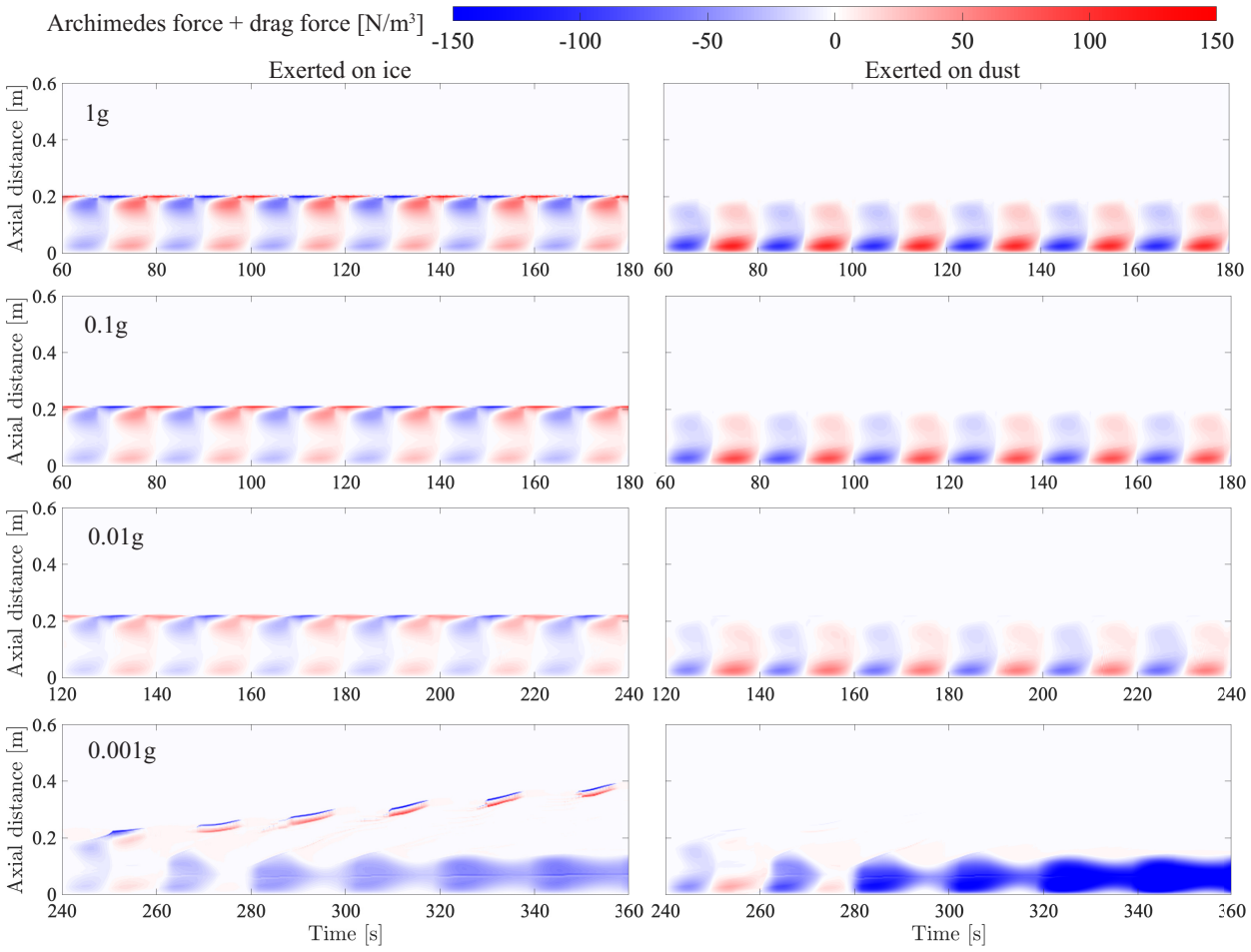

Figure 4.13: The summation of Archimedes force and drag force on ice and dust particles as a function of time for different gravity when the cyclic heat source is being applied. The sublimation and condensation are turned off.

changes periodically as the temperature changes cyclically. Therefore, the particles also move up and down with periodic variations in volume fractions. When gravity is stronger, the system has larger resistance to heat-induced forces, and the periodic variations become smaller.

When gravity is 0.001g, the magnitude of heat-induced forces is larger than the gravitational force. Heat-induced forces lift the ice from the ground and push the dust to the bottom, which leads to the further separation of ice and dust. Since there is more ice on the top of the pile and more dust at the bottom initially, the gas temperature is highest near the upper surface of the particle pile. As a result, the heat-induced forces are acting upward near the surface region (0.2m to 0.4m) and

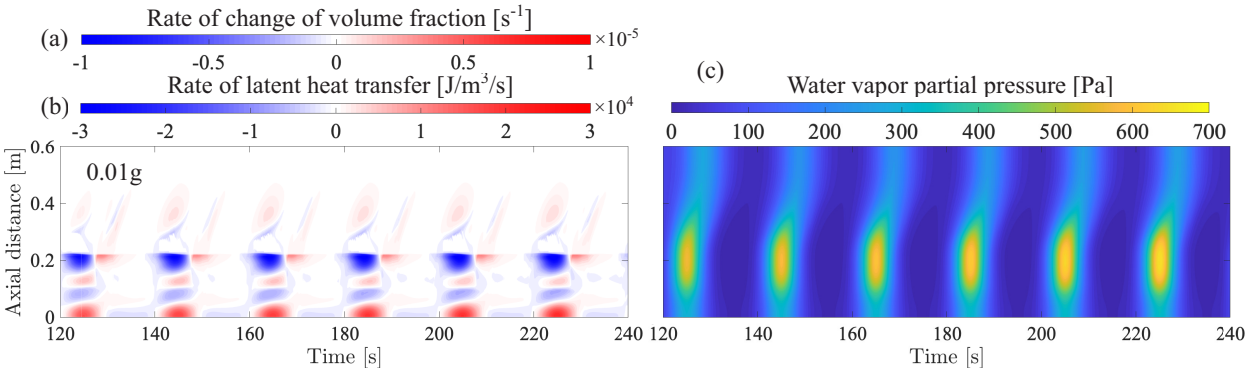

Figure 4.14: Computed profiles of (a) rate of change in ice volume fraction, (b) rate of latent heat transfer due to phase change, and (c) water vapor partial pressure in the case with 0.01g as the cyclic heat source being applied. (a) and (b) shares the same contour.

acting downward inside the particle pile (0 to 0.2m), and this causes the above particle behavior.

Now the role of phase change can be analyzed. Sublimation and condensation processes affect particle motion in three ways by considering how they: (1) change the local ice volume fractions directly, (2) change the local temperature through latent heat transfer, and (3) change the local water-vapor pressure. Among these three, (1) directly affects the number of particles, and (2) and (3) affect particle motions by adjusting the local gas temperature and pressure, which in turn modifies the heat-induced forces.

Fig. 4.14 shows the three effects during heating and cooling processes using the 0.01g case as an example. The change in local ice volume fraction is minimal compared to the total amount of ice since the integrated rate of change in one heating period is around 0.01%. The effect of latent heat transfer due to sublimation or condensation is also tiny compared to the magnitude of cyclic heat source. The local water-vapor pressure depends on the local saturation pressure, which is a function of only gas temperature. In the model problem, the gas temperature varies from 230K to 270K, and the water vapor pressure varies from 20Pa to 700Pa. Since the ambient air pressure is in the order of 1atm, the change in water vapor pressure is small compared to the change in gas pressure due to temperature variations. Nevertheless, as the major source of outgassing, the water vapor can lift the surface particles in low-pressure conditions [10]. In this case, the effect of phase

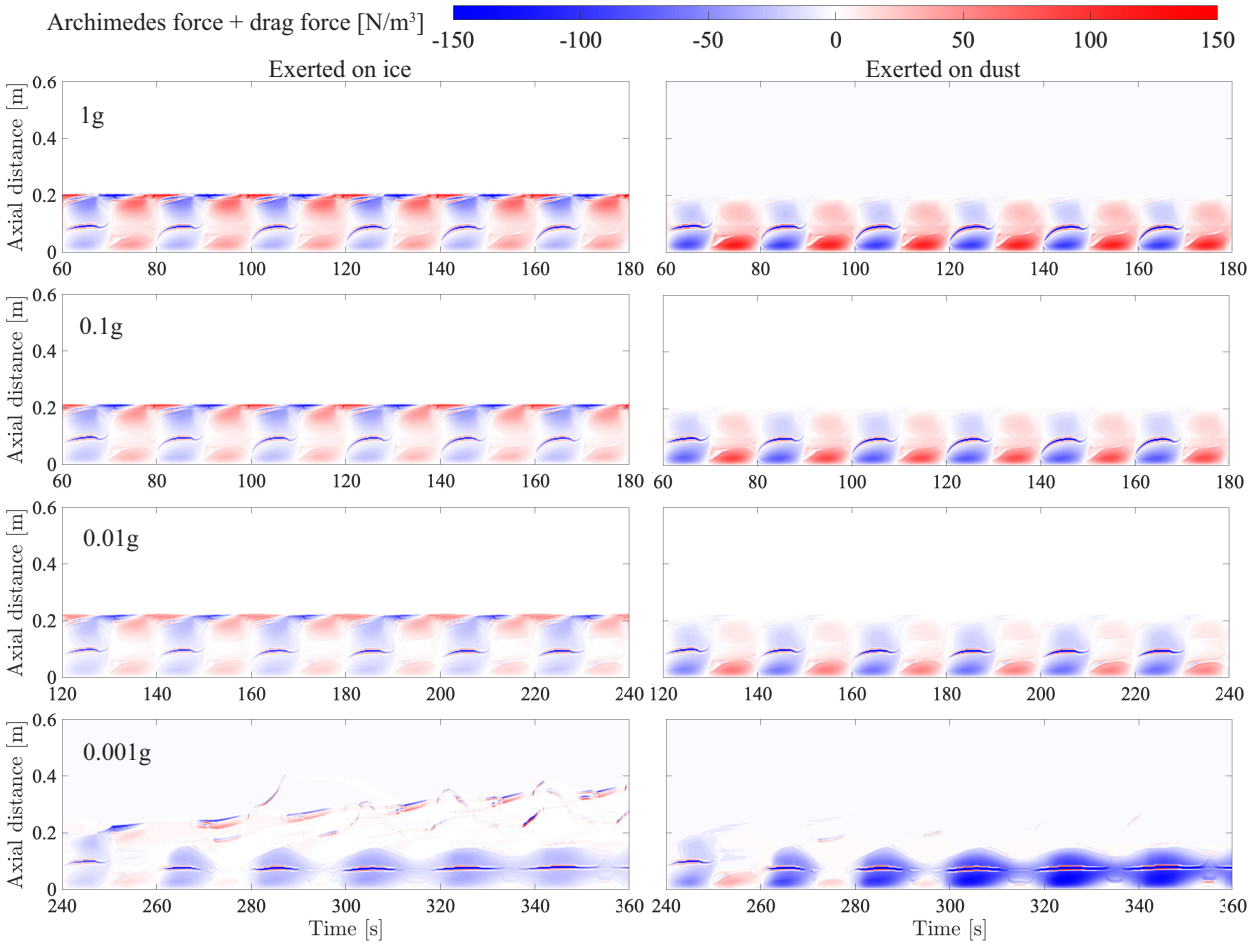

Figure 4.15: The summation of Archimedes force and drag force on ice and dust particles as a function of time under different gravity when the cyclic heat source is being applied. The sublimation and condensation processes are considered.

change on particle motion is small compared to the cyclic heat source.

The profiles of heat-induced forces considering the phase change mechanism are shown in Fig. 4.15. Compared to Fig. 4.13, large heat-induced forces can be found at the middle of the particle pile in all cases. In the 0.001g case, additional heat-induced forces are also generated near the region where the ice particles are drifted upward. These changes in heat-induced forces are caused by the sublimation and condensation processes as they modify the local gas temperature and pressure. Aside from these differences, the force profiles look similar to the case without phase change.

In general, the heat-induced forces, gravitational force, and intergranular stress force determine particle behavior. The intergranular stress force acts in reaction to other forces and only has a decelerating effect. The magnitude of heat-induced forces is independent of gravity. Therefore, particle motion depends on the magnitude of heat-induced forces and gravitational force, and whether the particles can be lifted depends on the cyclic heat source and gravity. When the heat-induced forces are stronger than the gravitational force, the particles can be lifted. Otherwise, the particles stay on the ground. In the given test cases, the ice particles are lifted and further separated from the particle mixture when the gravity is 0.001g. In addition, the phase change process shows a small effect on the magnitude of heat-induced forces in the given scenario. The results can be associated with the ice surface formation on T1, as discussed further below.

5. DISCUSSIONS

5.1 Result interpretations in terms of ice surface formation on T1

In section 4, we analyzed the ice and dust particle behavior in different gravities using force evaluations for two consecutive scenarios: (1) From an initial uniform mixture to a steady-state, and (2) From the steady-state with a cyclic heat source. Now, we answer the two questions related to the ice surface formation on T1 using the results presented above.

The particle behavior mainly depends on the balance among Archimedes force, drag force, intergranular stress force, and gravitational force. Before the system reaches a steady-state, the intergranular stress force and gravitational force are dominant. Due to the difference in density, the ice and dust are subject to different intergranular stress forces and gravitational forces, leading to the separation of ice on top of dust at the steady-state. Such particle behavior is related to the intergranular stress model, which will be addressed with detail in section 5.3. The steady-state could represent the static cometary surface.

When a cyclic heat source is applied, additional Archimedes force and drag force are generated, referred to as heat-induced forces. The intergranular stress force only has a secondary effect, and the particle behavior mainly depends on the magnitude of heat-induced forces and gravitational force. When the upward heat-induced forces are strong enough to overcome the gravitational force, the particles can be lifted from the ground. A significant result that links to the ice surface formation process is that the ice particles are lifted and further separated from dust under the effect of a cyclic heat source in very low gravity. This result could lead to an ice surface and thus support our hypothesis. The heat-induced forces are affected by two factors: (1) thermal expansion of local gases and (2) ice sublimation and condensation. It is found that thermal expansion plays a dominant role in the test problem, which, to our conjecture, is because of the large inert gas pressure. In addition, gravity does not affect the heat-induced forces, so particle lifting and further separation could occur more easily if the gravity is smaller

The gravity and temperature range in the 0.001g case are close to the estimated T1 conditions [2], but the gas conditions, period of external heat source, particle size and species, and simulation length scale are still far from reality. Analyzing the effects of these parameters is the next step of this study. The existing simulations give us insights into the physics and numerical issues of the problem, and they lay the foundation for future work. The rest of the discussion focuses on a brief parametric analysis and possible improvements on the multiphase model, which bring the simulations closer to T1 investigations.

5.2 Parametric analysis of the test problem

Now, we briefly discuss how other conditions can affect particle behavior and the further separation of ice and dust. These conditions include the amplitude and period of heat source, inert gas pressure, and particle size.

The amplitude and period of heat sources determine the range and rate of temperature variation, which control the magnitude of heat-induced forces. If the amplitude is smaller or the period is longer, the heat-induced forces are smaller so that the particle lifting and further separation can only occur with weaker gravity.

The amount of inert gas can influence thermal expansion, which changes the magnitude of heat-induced forces. Since the heat-induced forces are also affected by ice sublimation and condensation, a monotonic correlation is hard to find between heat-induced forces and the amount of inert gas. If the inert gas pressure is smaller, the ice outgassing will perform a more dominant role in the particle behavior, and the effect of thermal expansion will be more negligible.

Varying the particle size will affect the rate of phase change and the magnitude of the drag force. The rate of phase change is a function of particle diameter, as shown in Eq. (2.16). When the ice particle size is larger, the sublimation and condensation rate increases because the interface area between particles and gas increases. The drag force is smaller when the particle is larger according to Eq. (A.8), in which the gas-solid exchange coefficient K_{gl} is smaller when d_l is larger. If the particles of the same species have different sizes, ice particles or dust particles with different sizes need to be analyzed using additional sets of equations. A more detailed analysis of the effect of

particle size could be performed in the future.

5.3 Evaluation of the multiphase model

The results described above demonstrated the ability of this model to simulate essential physical processes involved in cometary surface evolution. Nevertheless, some components of this model need improvements or justifications to represent the processes on the cometary surface more accurately. These are now discussed in some detail.

5.3.1 Granular frictional pressure

The force balances between the intergranular stress force and gravitational force at the steady state can be simplified as,

$$\begin{cases} F_{ps,ice} = \frac{\partial p_{s,ice,tot}}{\partial x} = \alpha_{s,ice}\rho_{s,ice}g, \\ F_{ps,dust} = \frac{\partial p_{s,dust,tot}}{\partial x} = \alpha_{s,dust}\rho_{s,dust}g. \end{cases} \tag{5.1}$$

Because $p_{s,l,fric}$ is much larger than $p_{s,l}$ in densely packed regions [27], the granular frictional pressure provides the supportive force to balance the gravity, which is essential for maintaining a static packing state. Originally, the frictional pressure model was designed to provide extra intergranular stress in dense regions to limit compaction [27]. The applicability of this model to static packing problems has been questioned in a study of dense granular flow on an inclined surface using this frictional pressure model [40]. Several alternative expressions for the frictional pressure model also exist [41], and these should be tested.

If there is only one type of particle in the system, the static packing state represented by the current frictional pressure model is good enough. When there are multiple types of particles, the contact forces between different types of particles are poorly represented by the current model. Because $p_{s,l,fric}$ is a function of volume fractions, the force balances at the steady-state turn into two differential equations about the volume fractions of ice and dust. Therefore, the steady-state volume-fraction profile becomes directly correlated with the frictional pressure model. This means that given a different expression, the system may result in a different steady-state profile. In reality,

however, the static packing state should be independent of the model we are using. Moreover, there should be an infinite number of steady packing states when there are multiple types of particles. The current model can only demonstrate one steady-state profile, where ice particles accumulate on top of dust. We think this steady-state setup is acceptable and can still be used to analyze the surface evolution under the effect of cyclic heat sources. A better frictional pressure model needs to be constructed to remove the correlation between forces and local particle compositions, which will allow different cometary surface conditions to be represented.

5.3.2 Phase change and cyclic heat source

The phase-change model used here is valid under the assumption that the amount of ice does not change significantly due to sublimation, and sublimation does not affect the average particle diameter. On comets, it is frequently seen that all ice particles are sublimated, and the water vapor is released to outer space [10]. Therefore, calibrations are required to apply the phase change model to large-scale calculations where particle diameter varies significantly due to sublimation. In addition, this phase-change model does not include liquid water, which could be temporarily generated when the temperature is above the freezing point.

The cyclic heat source model in this work is a model of solar radiation. The linear heat distribution coefficient is an approximation to model the heat penetration. A better heat source model should consider the heat convection, conduction, and radiation processes through granular media. It is possible to learn from exiting heat radiation models for porous media [42] to build up a new cyclic heat model for a cometary surface.

5.3.3 Boundary conditions

In this work, we used adiabatic wall boundary conditions. The total mass of inert gas, water, and dust and the total energy are conserved in this system. In reality, the gas and particles should be allowed to leave or enter the domain, however, such boundary condition is hard to implement since we have limited knowledge of the external flow properties. We analyzed the effect of the upper wall boundary by performing the same simulation in different domain lengths. It is found

that the particle behavior inside the system is not affected by the height of the upper wall as long as there is no particle touching the boundary, in which case the particles are supposed to continue to rise.

5.3.4 Numerical method

For the calculations in this project, each 1D test required around 24 CPU-hour to finish by running serially on Intel Xeon 2.5GHz E5-2670 v2 processor. The different physical processes in the gas-solid flow system have a wide variety of time scales. The shortest time scale in the system is around 10^{-6}s, which appears in the integration of the drag force and the explicit hydrodynamic equations. The longest time scale is the period of cyclic heat source, which is 20s, and this value should be in the order of days in realistic cometary condition [2]. Therefore, the test problems end in millions of steps, which will be more expensive in large-scale, long-time multi-dimensional problems. In most coma simulations, the cell size is in the order of kilometers [15], which leads to much larger time steps in the explicit scheme with the cost of resolution. Using an implicit solver can also increase the shortest time scale in the system since it overcomes the acoustic limit of hyperbolic equations [43]. Evaluating these approaches to reduce the computational cost is a future topic of this study.

6. SUMMARY AND CONCLUSION

This thesis presents the first attempt at using a gaseous-granular multiphase model to describe gas, ice, and dust interactions with phase change and cyclic heat sources. The model is designed to simulate the processes controlling a cometary surface and prepare for the investigation of observed ice surfaces on T1. Several test problems using this model demonstrate the relative effects of gravity, heat sources, and phase change involved in the cometary surface evolution.

The steady-state results at different gravities show the static packing state of particles on the cometary surface. Ice and dust particles go through free-fall and separation stages and reach a steady-state where ice and dust are partially separated with ice on top of dust. The steady-state volume fraction profiles at different gravities are similar, but the particles are more densely packed when the gravity is stronger.

A cyclic heat source was applied to the steady-states to show the particle-lifting process. The cyclic heat source generates Archimedes and drag forces that cause particle motion. The magnitude of heat-induced forces is the same for different gravities. In test cases where the gravitational force is stronger, the particles experience periodic upward and downward motions while keep gravitationally bound to the cometary surface. When the magnitude of heat-induced forces is larger than the gravitational force, ice particles are lifted from the ground and further separated from the dust. Given the test conditions, the sublimation and condensation processes have only a small effect on the magnitude of the heat-induced forces.

In the 0.001g case, the separation of ice and dust could lead to an ice surface, which supports the ice surface formation hypothesis. The gravity and temperature range in this test are close to the actual conditions on T1, but the inert gas pressure, period of the heat cycle, length scale, particle sizes, and particle species are different from reality. A more detailed analysis should be done in the future to make the simulation closer to reality. In general, the current results provide the fundamental support of the theory of particle motion and can guide further exploration of physics and numerics.

7. FUTURE WORK

In this chapter, we list the future work of this project in detail. The next steps of this study can be generally divided into the following three aspects: (1) Conduct simulations of the ice-dust system in different conditions, length scales, time scales, and dimensions. (2) Improve the model components, including the granular frictional pressure model, the phase change model, and the cyclic heat source model to satisfy the requirements of deep analysis. (3) Improve the solver scheme, numerical implementation, and simulation setup to reduce the computational cost.

The quantities that characterize the system consist of gravity, inert gas pressure, amplitude and period of cyclic heat source, and densities and diameters of different particles. In this thesis, we have completed the analyses of ice-dust flow under different gravities only. The next step is to perform detailed parametric analyses of the system and generalize the particle behavior in other different conditions. We should also set up cases with various particle layer thicknesses to see if the particle behavior will be different if the amount of particles changes. Simulations can be conducted for a longer physical time to see if there is a maximum lifting height. 2D simulations, if affordable, should be conducted to see if any particle circulation occurs in the system, where particle lifting and deposition happen simultaneously at different locations.

Some model components should be improved for more accurate analysis. The current granular friction pressure model needs to be modified to remove the correlation between forces and local particle compositions. Additionally, more data is needed to verify the steady-state results calculated using this frictional pressure model when the ice and dust particle sizes are different. The phase change model should also consider the liquid phase since the temperature on T1 could exceed 273.15K. Calibrations are also needed if we consider the change in ice particle diameter during sublimation and condensation. The current cyclic heat source model is a significant simplification of cyclic solar radiation. If we keep this model, the heat distribution coefficient needs to be reconsidered carefully. Data for heat radiation through granular media can be studied to set up more accurate heat distribution coefficients or build new heat source models.

In order to conduct large-scale, multi-dimensional simulations of the cometary surface, the current numerical implementation, and simulation setup also need to be improved to increase the computational efficiency. Instead of keeping this explicit solver, we can try to build a multiphase implicit solver based on the existing Barely Implicit Correction (BIC) algorithm [43]. In this way, we can achieve much larger time steps so that longer simulations can be achieved for the same computational cost. Adaptive mesh refinement (AMR) should also be implemented to reduce the resolution at the background region. Eventually, the solver should be re-written in parallel (with GPU if possible) to run on supercomputers.

REFERENCES

[1] J. M. Sunshine, N. Thomas, M. R. El-Maarry, and T. L. Farnham, "Evidence for geologic processes on comets," *Journal of Geophysical Research-Planets*, vol. 121, no. 11, pp. 2194–2210, 2016.

[2] M. F. A'Hearn, M. J. S. Belton, W. A. Delamere, J. Kissel, K. P. Klaasen, L. A. McFadden, K. J. Meech, H. J. Melosh, P. H. Schultz, J. M. Sunshine, P. C. Thomas, J. Veverka, D. K. Yeomans, M. W. Baca, I. Busko, C. J. Crockett, S. M. Collins, M. Desnoyer, C. A. Eberhardy, C. M. Ernst, T. L. Farnham, L. Feaga, O. Groussin, D. Hampton, S. I. Ipatov, J. Y. Li, D. Lindler, C. M. Lisse, N. Mastrodemos, W. M. Owen, J. E. Richardson, D. D. Wellnitz, and R. L. White, "Deep impact: Excavating comet tempel 1," *Science*, vol. 310, no. 5746, pp. 258–264, 2005.

[3] M. C. De Sanctis, F. Capaccioni, M. Ciarniello, G. Filacchione, M. Formisano, S. Mottola, A. Raponi, F. Tosi, D. Bockelee-Morvan, S. Erard, C. Leyrat, B. Schmitt, E. Ammannito, G. Arnold, M. A. Barucci, M. Combi, M. T. Capria, P. Cerroni, W. H. Ip, E. Kuehrt, T. B. McCord, E. Palomba, P. Beck, E. Quirico, and V. Team, "The diurnal cycle of water ice on comet 67p/churyumov-gerasimenko," *Nature*, vol. 525, no. 7570, pp. 500–+, 2015.

[4] Y. Liao, R. Marschall, C. C. Su, J. S. Wu, I. L. Lai, O. Pinzon, and N. Thomas, "Water vapor deposition from the inner gas coma onto the nucleus of comet 67p/churyumov-gerasimenko," *Planetary and Space Science*, vol. 157, pp. 1–9, 2018.

[5] S. Fornasier, S. Mottola, H. U. Keller, M. A. Barucci, B. Davidsson, C. Feller, J. D. P. Deshapriya, H. Sierks, C. Barbieri, P. L. Lamy, R. Rodrigo, D. Koschny, H. Rickman, M. A'Hearn, J. Agarwal, J. L. Bertaux, I. Bertini, S. Besse, G. Cremonese, V. Da Deppo, S. Debei, M. De Cecco, J. Deller, M. R. El-Maarry, M. Fulle, O. Groussin, P. J. Gutierrez, C. Guttler, M. Hofmann, S. F. Hviid, W. H. Ip, L. Jorda, J. Knollenberg, G. Kovacs, R. Kramm, E. Kuhrt, M. Kuppers, M. L. Lara, M. Lazzarin, J. J. L. Moreno, F. Marzari,

M. Massironi, G. Naletto, N. Oklay, M. Pajola, A. Pommerol, F. Preusker, F. Scholten, X. Shi, N. Thomas, I. Toth, C. Tubiana, and J. B. Vincent, "Rosetta's comet 67p/churyumov-gerasimenko sheds its dusty mantle to reveal its icy nature," *Science*, vol. 354, no. 6319, pp. 1566–1570, 2016.

[6] H. U. Keller, S. Mottola, S. F. Hviid, J. Agarwal, E. Kuhrt, Y. Skorov, K. Otto, J. B. Vincent, N. Oklay, S. E. Schroder, B. Davidsson, M. Pajola, X. Shi, D. Bodewits, I. Toth, F. Preusker, F. Scholten, H. Sierks, C. Barbieri, P. Lamy, R. Rodrigo, D. Koschny, H. Rickman, M. F. A'Hearn, M. A. Barucci, J. L. Bertaux, I. Bertini, G. Cremonese, V. Da Deppo, S. Debei, M. De Cecco, J. Deller, S. Fornasier, M. Fulle, O. Groussin, P. J. Gutierrez, C. Guttler, M. Hofmann, W. H. Ip, L. Jorda, J. Knollenberg, J. R. Kramm, M. Kuppers, L. M. Lara, M. Lazzarin, J. J. Lopez-Moreno, F. Marzari, G. Naletto, C. Tubiana, and N. Thomas, "Seasonal mass transfer on the nucleus of comet 67p/chuyumov-gerasimenko," *Monthly Notices of the Royal Astronomical Society*, vol. 469, pp. S357–S371, 2017.

[7] I. L. Lai, W. H. Ip, J. C. Lee, Z. Y. Lin, J. B. Vincent, N. Oklay, H. Sierks, C. Barbieri, P. Lamy, R. Rodrigo, D. Koschny, H. Rickman, H. U. Keller, J. Agarwal, M. A. Barucci, J. L. Bertaux, I. Bertini, D. Bodewits, S. Boudreault, G. Cremonese, V. Da Deppo, B. Davidsson, S. Debei, M. De Cecco, J. Deller, S. Fornasier, M. Fulle, O. Groussin, P. J. Gutierrez, C. Guttler, M. Hofmann, S. F. Hviid, L. Jorda, J. Knollenberg, G. Kovacs, J. R. Kramm, E. Kuhrt, M. Kuppers, L. M. Lara, M. Lazzarin, J. J. Lopez-Moreno, F. Marzari, G. Naletto, X. Shi, C. Tubiana, and N. Thomas, "Seasonal variations in source regions of the dust jets on comet 67p/churyumov-gerasimenko," *Astronomy & Astrophysics*, vol. 630, 2019.

[8] N. Thomas, H. Sierks, C. Barbieri, P. L. Lamy, R. Rodrigo, H. Rickman, D. Koschny, H. U. Keller, J. Agarwal, M. F. A'Hearn, F. Angrilli, A. T. Auger, M. A. Barucci, J. L. Bertaux, I. Bertini, S. Besse, D. Bodewits, G. Cremonese, V. Da Deppo, B. Davidsson, M. De Cecco, S. Debei, M. R. El-Maarry, F. Ferri, S. Fornasier, M. Fulle, L. Giacomini, O. Groussin, P. J. Gutierrez, C. Guttler, S. F. Hviid, W. H. Ip, L. Jorda, J. Knollenberg, J. R. Kramm, E. Kuhrt, M. Kuppers, F. La Forgia, L. M. Lara, M. Lazzarin, J. J. L. Moreno, S. Magrin,

S. Marchi, F. Marzari, M. Massironi, H. Michalik, R. Moissl, S. Mottola, G. Naletto, N. Oklay, M. Pajola, A. Pommerol, F. Preusker, L. Sabau, F. Scholten, C. Snodgrass, C. Tubiana, J. B. Vincent, and K. P. Wenzel, "The morphological diversity of comet 67p/churyumov-gerasimenko," *Science*, vol. 347, no. 6220, 2015.

[9] N. Thomas, B. Davidsson, M. R. El-Maarry, S. Fornasier, L. Giacomini, A. G. Gracia-Berna, S. F. Hviid, W. H. Ip, L. Jorda, H. U. Keller, J. Knollenberg, E. Kuhrt, F. La Forgia, I. L. Lai, Y. Liao, R. Marschall, M. Massironi, S. Mottola, M. Pajola, O. Poch, A. Pommerol, F. Preusker, F. Scholten, C. C. Su, J. S. Wu, J. B. Vincent, H. Sierks, C. Barbieri, P. L. Lamy, R. Rodrigo, D. Koschny, H. Rickman, M. F. A'Hearn, M. A. Barucci, J. L. Bertaux, I. Bertini, G. Cremonese, V. Da Deppo, S. Debei, M. de Cecco, M. Fulle, O. Groussin, P. J. Gutierrez, J. R. Kramm, M. Kuppers, L. M. Lara, M. Lazzarin, J. J. L. Moreno, F. Marzari, H. Michalik, G. Naletto, J. Agarwal, C. Guttler, N. Oklay, and C. Tubiana, "Redistribution of particles across the nucleus of comet 67p/churyumov-gerasimenko," *Astronomy & Astrophysics*, vol. 583, 2015.

[10] R. Marschall, Y. Skorov, V. Zakharov, L. Rezac, S. B. Gerig, C. Christou, S. K. Dadzie, A. Migliorini, G. Rinaldi, J. Agarwal, J. B. Vincent, and D. Kappel, "Cometary comae-surface links the physics of gas and dust from the surface to a spacecraft," *Space Science Reviews*, vol. 216, no. 8, 2020.

[11] T. L. Farnham, D. Lampkin, J. M. Sunshine, E. S. Oran, and S. Lai, "Investigation of the smooth flows on the surface of comet tempel 1," *Grant proposal Submitted in response to NASA ROSES Solicitation NNH17ZDA001N-DDAP*.

[12] Y. Kitamura, "Axisymmetric dusty gas-jet in the inner coma of a comet .2. the case of isolated jets," *Icarus*, vol. 72, no. 3, pp. 555–567, 1987.

[13] A. Korosmezey and T. I. Gombosi, "A time-dependent dusty gas-dynamic model of axisymmetric cometary jets," *Icarus*, vol. 84, no. 1, pp. 118–153, 1990.

[14] J. F. Crifo, A. L. Itkin, and A. V. Rodionov, "The near-nucleus coma formed by interacting dusty gas jets effusing from a cometary nucleus .1.," *Icarus*, vol. 116, no. 1, pp. 77–112, 1995.

[15] J. F. Crifo, G. A. Lukianov, A. V. Rodionov, G. O. Khanlarov, and V. V. Zakharov, "Comparison between navier-stokes and direct monte-carlo simulations of the circumnuclear coma - i. homogeneous, spherical source," *Icarus*, vol. 156, no. 1, pp. 249–268, 2002.

[16] V. Tenishev, M. R. Combi, and M. Rubin, "Numerical simulation of dust in a cometary coma: Application to comet 67p/churyumov-gerasimenko," *Astrophysical Journal*, vol. 732, no. 2, 2011.

[17] G. Sarid, D. Prialnik, K. J. Meech, J. Pittichova, and T. L. Farnham, "Thermal evolution and activity of comet 9p/tempel 1 and simulation of a deep impact," *Publications of the Astronomical Society of the Pacific*, vol. 117, no. 834, pp. 796–809, 2005.

[18] D. Prialnik, M. F. A'Hearn, and K. J. Meech, "A mechanism for short-lived cometary outbursts at sunrise as observed by deep impact on 9p/tempel 1," *Monthly Notices of the Royal Astronomical Society*, vol. 388, no. 1, pp. L20–L23, 2008.

[19] S. N. P. Vegendla, G. J. Heynderickx, and G. B. Marin, "Comparison of eulerian-lagrangian and eulerian-eulerian method for dilute gas-solid flow with side inlet," *Computers & Chemical Engineering*, vol. 35, no. 7, pp. 1192–1199, 2011.

[20] Y. V. Skorov, L. Rezac, P. Hartogh, and H. U. Keller, "Is near-surface ice the driver of dust activity on 67p/churyumov-gerasimenko," *Astronomy & Astrophysics*, vol. 600, 2017.

[21] S. N. P. Vegendla, G. J. Heynderickx, and G. B. Marin, "Comparison of eulerian-lagrangian and eulerian-eulerian method for dilute gas-solid flow with side inlet," *Computers & Chemical Engineering*, vol. 35, no. 7, pp. 1192–1199, 2011.

[22] C. K. K. Lun, S. B. Savage, D. J. Jeffrey, and N. Chepurniy, "Kinetic theories for granular flow - inelastic particles in couette-flow and slightly inelastic particles in a general flowfield," *Journal of Fluid Mechanics*, vol. 140, no. Mar, pp. 223–256, 1984.

[23] D. Gidaspow, *Multiphase flow and fluidization : continuum and kinetic theory descriptions*. Boston: Academic Press, 1994.

[24] M. Syamlal, W. Rogers, and T. J. O'Brien, "Mfix documentation theory guide,"

[25] M. Pelanti and R. J. Leveque, "High-resolution finite volume methods for dusty gas jets and plumes," *Siam Journal on Scientific Computing*, vol. 28, no. 4, pp. 1335–1360, 2006.

[26] R. Saurel and R. Abgrall, "A multiphase godunov method for compressible multifluid and multiphase flows," *Journal of Computational Physics*, vol. 150, no. 2, pp. 425–467, 1999.

[27] R. W. Houim and E. S. Oran, "A multiphase model for compressible granular-gaseous flows: formulation and initial tests," *Journal of Fluid Mechanics*, vol. 789, pp. 166–220, 2016.

[28] N. G. Deen, M. V. Annaland, M. A. Van der Hoef, and J. A. M. Kuipers, "Review of discrete particle modeling of fluidized beds," *Chemical Engineering Science*, vol. 62, no. 1-2, pp. 28–44, 2007.

[29] M. J. Andrews and P. J. ORourke, "The multiphase particle-in-cell (mp-pic) method for dense particulate flows," *International Journal of Multiphase Flow*, vol. 22, no. 2, pp. 379–402, 1996.

[30] D. M. Snider, "An incompressible three-dimensional multiphase particle-in-cell model for dense particle flows," *Journal of Computational Physics*, vol. 170, no. 2, pp. 523–549, 2001.

[31] J. Dahal and J. A. McFarland, "A numerical method for shock driven multiphase flow with evaporating particles," *Journal of Computational Physics*, vol. 344, pp. 210–233, 2017.

[32] B. G. M. van Wachem, J. C. Schouten, C. M. van den Bleek, R. Krishna, and J. L. Sinclair, "Comparative analysis of cfd models of dense gas-solid systems," *Aiche Journal*, vol. 47, no. 5, pp. 1035–1051, 2001.

[33] S. Y. Lai, R. W. Houim, and E. S. Oran, "Effects of particle size and density on dust dispersion behind a moving shock," *Physical Review Fluids*, vol. 3, no. 6, 2018.

[34] S. Y. Lai, R. W. Houim, and E. S. Oran, "Mechanism and structure of subsurface explosions in granular media," *Physical Review Fluids*, vol. 2, no. 9, 2017.

[35] A. D. Thorpe and B. J. Mason, "Evaporation of ice spheres and ice crystals," *British Journal of Applied Physics*, vol. 17, no. 4, pp. 541, 1966.

[36] R. J. Schmidt, "Sublimation of wind-transported snow–a model," *USDA Forest Service research paper RM*, 1972.

[37] A. L. Buck, "New equations for computing vapor-pressure and enhancement factor," *Journal of Applied Meteorology*, vol. 20, no. 12, pp. 1527–1532, 1981.

[38] E. Jambon-Puillet, N. Shahidzadeh, and D. Bonn, "Singular sublimation of ice and snow crystals," *Nature Communications*, vol. 9, 2018.

[39] A. Kurganov and E. Tadmor, "New high-resolution central schemes for nonlinear conservation laws and convection-diffusion equations," *Journal of Computational Physics*, vol. 160, no. 1, pp. 241–282, 2000.

[40] P. F. Si, H. B. Shi, and X. P. Yu, "A general frictional-collisional model for dense granular flows," *Landslides*, vol. 16, no. 3, pp. 485–496, 2019.

[41] S. Schneiderbauer, A. Aigner, and S. Pirker, "A comprehensive frictional-kinetic model for gas-particle flows: Analysis of fluidized and moving bed regimes," *Chemical Engineering Science*, vol. 80, pp. 279–292, 2012.

[42] M. A. Gomez, D. Patino, R. Comesana, J. Porteiro, M. A. A. Feijoo, and J. L. Miguez, "Cfd simulation of a solar radiation absorber," *International Journal of Heat and Mass Transfer*, vol. 57, no. 1, pp. 231–240, 2013.

[43] X. Zhang, J. D. Chung, C. R. Kaplan, and E. S. Oran, "The barely implicit correction algorithm for low-mach-number flows," *Computers & Fluids*, vol. 175, pp. 230 – 245, 2018.

[44] H. L. Lu, Y. R. He, and D. Gidaspow, "Hydrodynamic modelling of binary mixture in a gas bubbling fluidized bed using the kinetic theory of granular flow," *Chemical Engineering Science*, vol. 58, no. 7, pp. 1197–1205, 2003.

[45] P. C. Johnson and R. Jackson, "Frictional-collisional constitutive relations for granular materials, with application to plane shearing," *Journal of Fluid Mechanics*, vol. 176, pp. 67–93, 1987.

[46] C. Wen and Y. Yu, "Mechanics of fluidization," *Chem. Eng. Prog. Symp. Ser.*, vol. 62, pp. 100–111, 1966.

[47] D. J. Gunn, "Transfer of heat or mass to particles in fixed and fluidized-beds," *International Journal of Heat and Mass Transfer*, vol. 21, no. 4, pp. 467–476, 1978.

[48] D. L. Koch and A. S. Sangani, "Particle pressure and marginal stability limits for a homogeneous monodisperse gas-fluidized bed: kinetic theory and numerical simulations," *Journal of Fluid Mechanics*, vol. 400, pp. 229–263, 1999.

APPENDIX A

DETAILS OF PHYSICAL MODEL

The intergranular stress $p_{sl,tot}$ is defined as the sum of granular pressure $p_{s,l}$ and frictional pressure $p_{fric,l}$,

$$p_{sl,tot} = p_{s,l} + p_{fric,l}. \tag{A.1}$$

where $p_{s,l}$ represents the collisional effects of the particles, and $p_{fric,l}$ represents the frictional effects between particles at densely packed regions. $p_{s,l}$ is defined as [44]

$$p_{s,l} = \alpha_{s,l}\rho_{s,l}\theta_{s,l} + \sum_{m=1}^{N_s} p_{c,lm}, \tag{A.2}$$

where $p_{c,lm}$ is the collisional pressure between particle l and m. $p_{c,lm}$ is defined as [44]

$$p_{c,lm} = \frac{\pi(1+e)d_{lm}g_{o,lm}n_l n_m m_l m_m m_0 \theta_{s,l}\theta_{s.m}}{3(m_l^2\theta_{s,l} + m_m^2\theta_{s,m})} \times \left[\frac{m_0^2\theta_{s,l}\theta_{s,m}}{(m_l^2\theta_{s,l} + m_m^2\theta_{s,m})(\theta_{s,l}+\theta_{s,m})}\right]^{3/2} \times (1 - 3\Delta + 6\Delta^2 - 10\Delta^3),$$

$$\begin{aligned} d_{lm} &= \frac{d_l + d_m}{2},\ m_0 = \frac{m_l + m_m}{2},\ \text{and} \\ \Delta &= \frac{m_l\theta_{s,l} - m_m\theta_{s,m}}{[(m_l^2\theta_{s,l}^2 + m_m^2\theta_{s,m}^2) + \theta_{s,l}\theta_{s,m}(m_l^2 + m_m^2)]^{1/2}}, \end{aligned} \tag{A.3}$$

where d_l is the particle diameter. e is the coefficient of restitution. In this model, e is taken as 0.01, where smaller e stands for more cohesive particles. n_l is the number of particles and m_l is the mass of one single particle. For spherical particles,

$$m_l = \frac{\pi}{6}d_l^3\rho_{s,l} \ \text{ and } \ n_l = \frac{6\alpha_{s,l}}{\pi d_l^3}. \tag{A.4}$$

$g_{0,lm}$ is the radial distribution function, which represents the probability of collision between particle tyle l and m. For a mixture of hard spheres, $g_{0,lm}$ is given as [33],

$$g_{0,lm} = \frac{1}{\alpha_g} + \frac{3 d_l d_m}{\alpha_g^2 (d_l + d_m)} \sum_{q=1}^{N_s} \frac{\alpha_{s,q}}{d_q}. \tag{A.5}$$

The frictional pressure $p_{fric,l}$ is essential for preventing the particle volume fraction from growing unphysically high at densely packed regions. The equation for $p_{fric,l}$ is developed by Johnson and Jackson [45] and modified by Lai [33] based on the law of partial pressure,

$$p_{fric,l} = \begin{cases} 0 & \text{if} \quad \alpha_{s,tot} < \alpha_{s,crit}, \\ Fr \frac{(\alpha_{s,tot} - \alpha_{s,crit})^2}{(\alpha_{s,max} - \alpha_{s,tot})^5} \alpha_{s,l} & \text{if} \quad \alpha_{s,tot} \geq \alpha_{s,crit}, \end{cases} \tag{A.6}$$

where $\alpha_{s,tot}$ is the total granular volume fraction, $\alpha_{s,max}$ is the packing limit, and $\alpha_{s,crit}$ is the critical value of total granular volume fraction for dense regions. Fr is a constant and is taken as 0.1N/m^2. For a mixture of spherical particles with the same diameter, $\alpha_{s,max}$ is 0.65. In this model, $\alpha_{s,crit}$ is set as 0.5.

The drag force between gas and particles, $f_{drag,gl}$, results from the velocity difference between gas and granular phase. The drag correlation is developed by Gidaspow [23],

$$f_{drag,gl} = K_{gl}(v_{s,l} - v_g), \tag{A.7}$$

where K_{gl} is the gas-solid exchange coefficient. K_{gl} is formulated based on the model of Wen & Yu for $\alpha_g > 0.8$ [46] and the Ergun equation for $\alpha_g \leq 0.8$ [23],

$$K_{gl} = \begin{cases} 0.75 C_{d,l} \frac{\rho_g \alpha_g \alpha_{s,l} |v_{s,l} - v_g|}{d_l \alpha_g^{2.65}} & \text{if } \alpha_g \geq 0.8, \\ 150 \frac{\alpha_{s,l}^2 \mu_g}{\alpha_g d_l^2} + 1.75 \frac{\rho_g \alpha_{s,l} |v_{s,l} - v_g|}{d_l} & \text{if } \alpha_g < 0.8, \end{cases} \tag{A.8}$$

where $C_{d,l}$ is the drag coefficient,

$$C_{d,l} = \begin{cases} 24(\alpha_g Re_l)^{-1}\left[1 + 0.15(\alpha_g Re_l)^{0.687}\right] & \text{if } \alpha_g Re_l < 1000, \\ 0.44 & \text{if } \alpha_g Re_l \geq 1000, \end{cases} \tag{A.9}$$

where Re_l is the Reynolds number, which is defined as

$$Re_l = \frac{\rho_g |v_{s,l} - v_g| d_l}{\mu_g}, \tag{A.10}$$

where μ_g is the gas dynamic viscosity.

The particle-hindrance force represents the resistence of relative motion between two types of particles. A model that is similar to the drag force is developed for $f_{drag,lm}$ [23],

$$f_{drag,lm} = K_{lm}(v_{s,l} - v_{s,m}), \tag{A.11}$$

where K_{lm} is the solid-solid exchange coefficient between particle type l and m [33],

$$K_{lm} = \frac{3(1+e)\left(\frac{\pi}{2} + C_{fr,lm}\frac{\pi^2}{8}\right)\alpha_{s,l}\rho_{s,l}\alpha_{s,m}\rho_{s,m}(d_l + d_m)^2 g_{0,lm}}{2\pi(\rho_{s,l}d_l^3 + \rho_{s,m}d_m^3)}|v_{s,l} - v_{s,m}|, \tag{A.12}$$

where $C_{fr,lm}$ is the friction coefficient between the two types of particles. In this model, we assume $C_{fr,lm} = 0$ and the friction between different types of particle are neglected.

The quantity $q_{conv,gl}$ stands for the convective heat transfer between gas and particles, which is dependent on their temperature difference,

$$q_{conv,gl} = 6\frac{\alpha_{s,l}\lambda_g Nu_l}{d_l^2}(T_g - T_{s,l}), \tag{A.13}$$

where Nu_l is the Nusselt number, which is estimated using the correlation by Gunn [47],

$$Nu_l = (7 - 10\alpha_g + 5\alpha_g^2)(1 + 0.7Re_l^{0.2}Pr_g^{1/3}) + (1.33 - 2.4\alpha_g + 1.2\alpha_g^2)Re_l^{0.7}Pr_g^{1/3}. \tag{A.14}$$

The quantity λ_g is the gas thermal conductivity and Pr_g is the gas phase Prandtl number.

The quantity $\phi_{visc,gl}$ represents the energy transfer between granular PTE and gas sensible energy due to viscous damping. The model for $\phi_{visc,gl}$ is developed by Gidaspow as [23]

$$\phi_{visc,gl} = 3K_{gl}\theta_{s,l}. \tag{A.15}$$

The quantity $\phi_{slip,gl}$ represents the production of granular PTE due to frictional heating between gas and particles. It is given by Koch and Sangani as [48]

$$\phi_{slip,gl} = \frac{81\alpha_{s,l}\mu_g^2}{g_0 d_l^3 \rho_{s,l}\sqrt{\pi}} \frac{|v_{s,l} - v_g|^2}{\sqrt{\theta_{s,l}}}. \tag{A.16}$$

The quantity $\dot{\gamma}_l$ represents the dissipation of PTE due to collisions between particles. The model used here is developed by Lun $et\ al.$ [22],

$$\dot{\gamma}_l = \frac{12(1-e^2)g_{0,ll}\alpha_{s,l}^2}{\sqrt{\pi}} \frac{\rho_{s,l}\theta_{s,l}^{3/2}}{d_l}. \tag{A.17}$$